SPIN SCATTERING IN SUPERCONDUCTORS

by

Larry John Williams

A Dissertation Submitted to the
Graduate Faculty in Partial Fulfillment of
The Requirements for the Degree of
DOCTOR OF PHILOSOPHY

Major Subject: Physics

Approved:

Signature was redacted for privacy.

In Charge of Major Work

Signature was redacted for privacy.

Head of Major Department

Signature was redacted for privacy.

Dean of Graduate College

Iowa State University
Ames, Iowa

1969

TABLE OF CONTENTS

INTRODUCTION

A fundamental feature of superconductivity is the cooperative character of the motion of the electrons in the metal. In the normal phase of a metal an independent particle picture (1) seems to describe rather well the way electrons interact with the lattice and impurities. In the superconducting phase, however, there are long range correlations in the spin and momentum states of the electrons (2) which drastically alter the way in which electrons interact with the lattice and impurity atoms and these long range correlations then are a central feature in zero resistance and the other superconducting properties. In many ways this cooperative superconducting phase of the electron gas is similar to an enormous molecule (3) in that the electron gas acts as a unit rather than as individual particles.

Complete discussions of the theory of superconductivity by Bardeen, Cooper, and Schieffer (BCS) and its extensions have been given elsewhere (2, 3, 4, 5, 6) so a brief outline of the relevant parameters will suffice here. Our present picture of the superconducting ground state of a metal is that the wave function is composed of a coherent mixture of normal state wave functions. For example, within the original BCS theory the normal state wave functions are taken to be Bloch states and the superconducting ground state is a very special mixture of these Bloch states which arises

through the coherent exchange of virtual phonons by the electrons. This mixture of Bloch states then forms a wave which has a configuration space dimension, ξ_o, of about 10,000 Å for typical electron densities in metals. A detailed calculation shows in fact that the lowest energy state for the system arises when electrons with wave vector $\vec{k}$ and spin up $(\vec{k}\uparrow)$ are exactly paired with other electrons of opposite wave vector and spin $(-\vec{k}\downarrow)$. That is, if state $(\vec{k}\uparrow)$ is occupied then $(-\vec{k}\downarrow)$ is also occupied and if $(\vec{k}\uparrow)$ is empty, then $(-\vec{k}\downarrow)$ is empty.

In a real metal, with all its impurities and defects, the normal state wave functions are more complicated than the simple Bloch states of BCS and in this situation Anderson (7) has pointed out that each normal state wave function is to be paired with its time-reverse wave function. For the BCS theory $(\vec{k}\uparrow)$ is the time reverse of $(-\vec{k}\downarrow)$ so the Anderson pairing is a natural extension of BCS. The existence of these pair state correlations in superconductors has received strong experimental verification from flux quantization and Josephson tunneling and they form the basis of our understanding of this whole subject.

In addition to the superconducting pair correlations in a metal, there may be other correlations arising from quite different effects. For example a ferromagnet, such as Gd or Fe, has an alignment of the moments and as a

result there is a spontaneous magnetization. As yet, the theories of ferromagnetism are not as well established as the theory of superconductivity but there is little doubt that spin correlations will be important in the final picture. Presumably one could have both superconducting and ferromagnetic (antiferromagnetic) spin correlations in the same metal and the electronic structure would reflect a competition between these two effects. The purpose of the work presented here is to study the effect of magnetic scattering on superconductivity and to study the interrelation of ferromagnetism and superconductivity.

The interesting question of how the presence of localized magnetic impurities affects these correlations was first examined experimentally by Matthias and co-workers in 1958 (8). They measured the reduction of the superconducting critical temperature, T_c, in La as a function of adding 1% of each of the other rare earth elements and found that a drastic lowering in T_c occurred which correlated with the spin of the impurity atom and not its total effective magnetic moment as might be expected. Additional measurements on other alloy systems (9) further demonstrated the essential dependence of the effect on impurity spin. Herring (10) and also Matthias and Suhl (11) advanced the idea that the effect was a result of an exchange interaction between the 4f spins and the conduction electrons.

In 1961 Abrikosov and Gor'kov (AG) (12) presented a rather complete theory of the effect of paramagnetic impurities on the superconducting properties of these alloys. The essential feature of this calculation is that the pair states have finite lifetimes as a result of spin flip scattering. It is especially important here to note the distinction between magnetic and non-magnetic impurities. The infinite lifetime "Cooper pair" states of BCS theory are not shortened or changed in any essential way by "potential" or non-magnetic scattering but they are strongly effected by scattering which destroys time reversal symmetry such as spin flip scattering. Very general arguments due to Anderson (7) demonstrate that infinite lifetime pair states with complete time reversal symmetry can be formed from the eigenstates obtained by first solving the potential scattering problem and then constructing the superconducting ground state. The addition of a magnetic scattering term[1] removes the invariance of the Hamiltonian under time reversal and a lifetime effect is introduced.

This lifetime (τ_s) effect results in an energy broadening ($\Gamma \simeq \frac{\hbar}{\tau_s}$) of states into the superconducting energy gap which then allows the possibility of substantially different superconducting characteristics. The most immediate and

---

[1] Maki and Fulde (13) have shown the equivalence of different pair-breaking mechanisms in superconductors.

obvious change is in the excitation spectrum near the Fermi surface where lifetime broadening has the largest effect. It can, in fact, lead to superconductivity even when there is no energy gap in the excitation spectrum. This is in contrast to the BCS case in which there are pair correlation and the energy gap at all temperatures. The phenomenon of "gaplessness" was especially important in that it showed that the condensation phenomenon and pair correlation were of primary importance in explaining the superconducting phase transition rather than the existence of an energy gap in the quasi-particle excitation spectrum.

Experimental verification of the theory for some systems is very good in cases where the impurity spins are uncorrelated (paramagnetic). AG theory has successfully predicted the T_c/T_{cp} vs n/n_{cr} curves. Maple (14) measured transition temperatures of the $La_{1-x}\ Gd_x\ Al_2$ system and found agreement all the way out to 90% of the critical concentration. His susceptibility measurements on the same system indicated $1/\chi$ was linear in T with an extrapolated Curie temperature less than 0.1 K. AG is in agreement with many other systems in the limit of small n, but shows disagreement near n_{cr}. This has been attributed to correlations among the impurity spins. Tunneling measurements by Reif and Woolf (15) also have shown the disappearance of the gap and agree with the AG density of states when properly

interpreted. A very precise set of tunneling measurements by Tinkham and Millstein (16) showed close agreement when electron mean free paths effects had been included. In addition, Decker (17) found the critical field curves of the Th-Gd system to be in agreement with AG (as extended by Skalski, Betbeder-Matibet, and Weiss (18)) to an accuracy of 0.5%. Extensions of AG theory to calculate transport properties (18, 19, 20, 21) have shown excellent agreement with experiment also (22). Of particular interest for this work is the agreement of Ambegaokar and Griffin's (20) calculation of thermal conductivity and the measurement of K_s/K_n for the Th_{1-x} Gd_x system (using Decker's samples) by Cappelletti (23). On the basis of this evidence one can only conclude that AG is an excellent description of BCS superconductors with paramagnetic impurities.

On the other hand the paramagnetic case is not the whole story. Superconducting alloy systems which show impurity spin correlations are also very common (24, 25, 26, 27, 28) and offer a whole new aspect of the problem. Matthias and co-workers (8, 25) have presented data on La_{1-x} Gd_x alloys in which the T_c/T_{cp} $\underline{vs}$ n/n_{cr} curve appears to intersect a magnetic order curve. They identified the ordering as ferromagnetic because a remanent magnetization was observed. However Finnemore and Hopkins (29) argued that the ordering was more nearly characteristic of

antiferromagnetism from a detailed study of the shape of the magnetization curves. In either case, all the moments in the sample are ordering in some fashion because there is an excess specific heat equal to nR ln 8 (29, 30).

The existence of impurity spin correlations appears in the form of deviations from the AG T_c/T_{cp} *vs* n/n_{cr} curve. The data of Crow and Parks (27) on La_{3-x} Gd_x In show a sharp increase in T_c with increasing Gd concentration (at about 0.8 n_{cr} where n_{cr} = 2.15 at.% Gd) followed by a rapid drop to zero at about 0.9 n_{cr}. The data of Matthias *et al*. (25) on La_{1-x} Gd_x show that T_c rises a slight amount over a wider range of impurity followed by a rapid drop to zero at about n = 1.4 at % Gd. The point at which the susceptibility deviates from the Curie law occurs at a much higher temperature than does the peak in the susceptibility. The deviation indicates the beginning of impurity spin correlations. If one plots these temperatures on the same graph with T_c/T_{cp} *vs* n/n_{cr} the paramagnetic spin correlation curve intersects the T_c curve at approximately the point where the anomalous behavior begins.

On the theoretical side, Gor'kov and Rusinov (31) proposed a theory to explain these systems based on a static exchange interaction between impurity spins. Bennemann (32, 33) extended their theory by using a time dependent exchange interaction between the conduction electrons and

the magnetic impurities. He was able to show reasonable qualitative agreement with the T_c/T_{cp} vs n/n_{cr} curves of Matthias (25) on La-Gd and Parks on La_{3-x} Gd_x In (27). In fairly simple terms the anomalous behavior can be understood by realizing that if the impurity spins order it becomes more difficult to spin flip scatter a conduction electron because the impurity spins become correlated with other spins and are less free to rotate. The reduced spin flip scattering enhances superconductivity resulting in the sharp increase in T_c vs n in the La_{3-x} Gd_x In system and the gentle increase in the La_{1-x} Gd_x system. At the same time the spin flipping is being reduced the exchange fields responsible for the ordering cause Zeeman splitting of the pair states at the Fermi surface. This effect is destructive to superconductivity and results in T_c going rapidly to zero. Spin orbit scattering can moderate this internal field effect because it mixes spin up and spin down states in normal state wave functions. Hence various amounts of spin-orbit scattering in the host material can alter the shape of the T_c vs concentration curve substantially near n_{cr}. This explains why higher concentrations are possible in the La_{1-x} Gd_x before the Zeeman splitting drives T_c to zero. Although the qualitative agreement is good the theory could be improved if more were known about the nature of the magnetic order.

A number of theoretical conjectures have been made

about the impurity spin correlations in the superconducting state. Anderson and Suhl (34) proposed a "cryptoferromagnetic" model in which the alignment is ferromagnetic over extremely small domains, on the order of 50 Å. Averaged over a coherence length however the net polarization is nearly zero. Their argument is based on the concept of a non-local susceptibility (different in the normal and superconducting states) which leads to a positive short range Ruderman-Kittel (35, 36, 37) interaction and a negative long range interaction. A different model proposed by Liu (38) argues toward a similar short range correlation (on the order of the nearest neighbor distance) but his argument is based on the nature of the Ruderman-Kittel interaction and the random space distribution of impurity spins. He argues that the ordering is basically the same as manganese in copper (39).

Klein and Brout (40, 41, 42) and also Marshall (43) were able to explain the low temperature specific heat and magnetic susceptibility of these very dilute Cu-Mn alloys with a detailed statistical model. Liu (44) extended the theory to more concentrated alloys. This version of the theory shows qualitative agreement with the La_{1-x} Gd_x susceptibility curves of Finnemore and co-workers (45).

Benneman, Garland, and Mueller (46) have recently attempted to explain the magnetic order in superconducting

dilute rare earth alloys by using the behavior of the upper critical magnetic field, H_{c2} (n,T). They are lead to the conclusion that the magnetic structure is not long range ferromagnetism nor long range uniform antiferromagnetism nor only short range order. They argue the data is consistent with ferrimagnetic spin clusters with spiral coupling to each other.

The brief discussion above should indicate that magnetic order coexisting with superconductivity is not well understood and for that reason a single crystal neutron diffraction experiment and a series of thermal conductivity experiments were undertaken. All of the experimental studies on this problem with the exception of the specific heat measurements of Phillips (30) and also Finnemore (29) have only given information at or above T_c. Both neutron diffraction and thermal conductivity provide data on ordering in superconductors at all accessible temperatures above and below T_c.

A calculation by Bennemann and Mueller (47) predicts an anomalous temperature dependence of the electronic thermal conductivity in the presence of ordering. Figure 1 which is taken from Bennemann's paper (47) can be understood in terms of the mechanisms previously discussed in connection with the anomalous behavior of T_c/T_{cp} vs n/n_{cr}. The dashed line represents the case of no impurity spin correlations (AG theory applies). The solid curve at the top shows

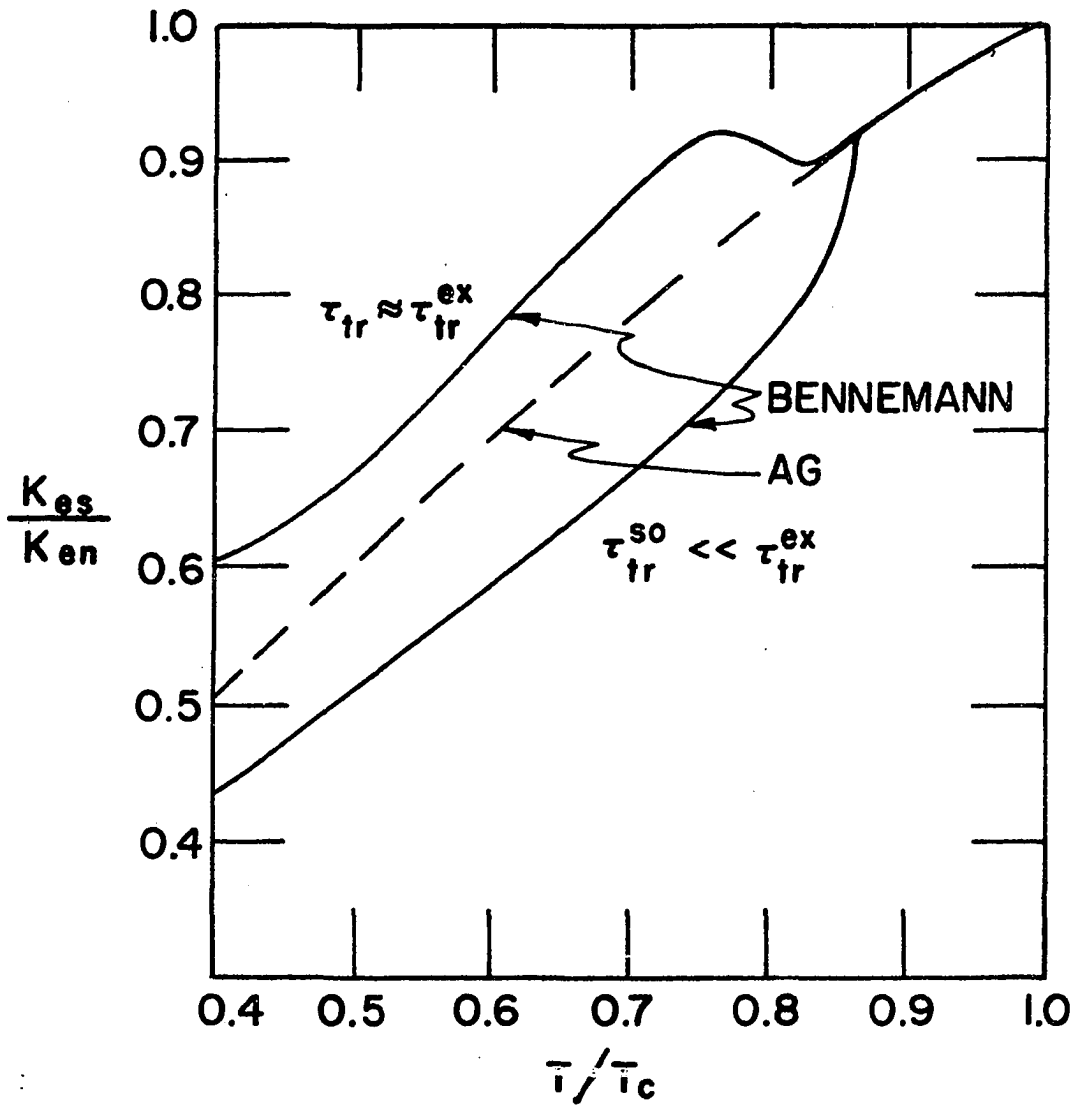

Figure 1. Anomalous temperature dependence of K_{es}/K_{en} which arises from the ordering of magnetic impurities. The details of the calculation are given by Bennemann (47).

the effect of the increased pair breaking which results from magnetic impurity exchange fields while the lower solid curve is predicted when the internal field effect is moderated by spin orbit scattering.

A determination of the electronic thermal conductivity is made difficult due to the presence of a fairly large lattice contribution. However more information is obtained about the superconducting order parameter by thermal conductivity measurements even in the presence of a confusing phonon term than can be obtained from specific heat data due to the presence of a large entropy term resulting from the magnetic ordering. La rare earth alloys are very useful in this type of study because La, having no 4f electrons, is the only rare earth element known to be a superconductor and the uncompensated 4f spins of the other rare earths (except for Lu) provide them with a localized magnetic moment. The chemical similarity which results from having the same outer electronic structure simplifies the problem considerably due to the minimization of valence effects, changes in the effective electron-electron interaction and distortions of the phonon spectrum at larger concentrations (48). At the same time the metallurgical considerations in sample fabrication are simpler due to the chemical similarity of the rare earths although La presents problems all its own as will be discussed later.

La_{80} Lu_{20-x} Tb_x rather than La_{1-x} Tb_x was chosen for single crystal neutron diffraction studies because the addition of Lu makes it possible to grow single crystals. Gd would have been preferable as the magnetic impurity because it has no orbital moment but it has a neutron absorbtion cross section three orders of magnitude larger than Tb. It was not possible to use the same system for thermal conductivity measurements since initial measurements showed the phonon contribution to be a factor of two or three larger than the electronic contribution at $T \sim 1/2\ T_c$. The La_{98} Lu_{2-x} Tb_x system retains a phonon contribution but other phonon scattering mechanisms seem to be present in this system which were not present in the other alloys so that the phonon conduction was less important. Although the phonons present the major obstacle in interpreting the data, information can still be obtained.

NEUTRON DIFFRACTION

The results of the single crystal as well as polycrystalline neutron diffraction experiments and susceptibility measurements are described in detail elsewhere (45) so only the results will be mentioned here.

The first neutron measurements on polycrystalline La_{90} Tb_{10} at low temperatures showed a broad peak characteristic of short range order in the impurity spin system. Similar features were observed in La_{80} Tb_{20} with the peak having the same width and correspondingly higher intensity. The range of the order seemed to be about the same in both alloys. Qualitatively these results are consistent with susceptibility studies in that the short range order peak appears at the same temperature at which the susceptibility curves break away from the Curie-Weiss law. The single crystal neutron diffraction measurements on La_{80} Lu_{15} Tb_5, however, failed to show the presence of any long or short range magnetic order. In fact the short range order peak, if present, was at least 200 times less intense in this sample than it was in the samples with 10 and 20 atomic percent Tb. The paramagnetic scattering did not change by more than 10 percent as the temperature was lowered through the susceptibility maximum (T_M) down to $T_M/2$.

Differential susceptibility measurements on a single crystal of La_{80} Lu_{15} Tb_5 (the Lu stabilizes the d-hcp phase

allowing single crystals to be grown) showed peaks in the a-axis and b-axis susceptibilities at about 5.7 K while the c-axis susceptibility was much smaller. This suggests that the moments are held in the basal plane by anisotropy fields. These results seem to indicate that the magnetic ions line up with respect to some local field with the full Tb moment randomly oriented in the basal plane.

THERMAL CONDUCTIVITY

Experimental Details

Sample preparation

The samples for thermal conductivity measurements were prepared by arc melting appropriate amounts of the pure rare earth metals, which were furnished by Professor Spedding's group of this laboratory. The impurities present in these starting materials in parts per million (ppm) by weight are shown in Table 1. Since the amounts of Lu and Tb in the final melt were small, master alloys of La-Tb and La-Lu were prepared before the final meltings. Table 2 shows the fractions used in calculating the number of grams of each constituent needed to obtain the atomic percent composition indicated. It assumes the atomic masses of La, Lu, and Tb to be 138.91, 174.97, and 158.924 respectively.

The procedure in each of the six metals was to cut about 30 grams of pure La from the starting ingots. This was electropolished until the surface was shiny using a perchloric acid methanol solution (49). The La was weighed to the nearest 0.1 mg and the weights of the other materials necessary to give the desired concentration were calculated for this weight. These Lu and Tb pieces were then cut and filed until the final weight was approximately reached. They were electropolished and then carefully brought to within 1 mg

Table 1. Impurities (in ppm by wt.) in starting materials (blank spaces indicate no test was run for the material listed)

	La	Lu	Tb
H	18	12	5
C	40		8
N	193	22	2
O	219	243	139
F	70		7
Mg	1	10	≤20
Al	1	10	8
Si	2	10	≤0.9
Ca	1	30	2
Cr	1	≤10	4
Fe	10	≤30	20
Ni	1	10	<70
Cu	1	10	20
Ta	20	≤200	6
W	≤100		
Sc	≤5	5	30
Y	<100	≤10	19
Ce	10		4.4
Pr	30		2.2
La			3.2
Nd	10		4.0
Sm	≤0.6		<0.8
Eu	≤2		<0.2
Gd	≤1		33
Tb	≤3		
Dy	8		10
Ho	2		20
Er	1	10	22

Table 1 (Continued)

	La	Lu	Tb
Tm	4	10	1.1
Yb	<1	<<100	<1
Lu	4		4

Table 2. Weight composition of the alloys

	Grams Lu / Grams La	Grams Tb / Grams La	Grams $La_{80}Lu_{20}$ / Grams La	Grams $La_{80}Tb_{20}$ / Grams La
Master Alloy 1 $La_{80}Lu_{20}$	.31490			
Master Alloy $La_{80}Tb_{20}$		.28602		
Sample 1 $La_{98}Lu_{02}$			.11688	
Sample 2 $La_{98}Lu_{1.15}Tb_{.85}$			.067206	.0485829
Sample 3 $La_{98}Lu_{1}Tb_{1}$			.058440	.057156

of the final weight by filing. Emission spectroscopy showed samples 1 and 2 to have a faint trace of Fe contamination. It is possible that the use of a stainless steel cathode for electropolishing is the source of the contamination. A platinum electrode should be used in the future.

The pieces were then placed in a copper mold, which had been previously cleaned with a 50% nitric acid solution, and placed in a standard arc-melter. The system was outgassed for 30 minutes at about 85^{o}C and flushed with He gas four or five times. The melting chamber was then bled up to a pressure of about 0.8 atmosphere with He. To further reduce the O_2 in the system a Zr button was melted three or four times just before the sample was melted. Since the Lu, Tb, and the master alloys melt at a higher temperature than pure La, they were always placed on top of the piece of La so they would melt first. The resultant button was then flipped and remelted a total of ten times to insure homogeneity. The whole button was then melted into a finger shaped mold 1/4" wide by 3" long and removed.

The finger was glued to a piece of brass with conducting glue and spark cut into a piece about 3 inches long with square cross section 0.14 x 0.14 inches. The carbonized surface of the sample, which arose during the spark cutting, was removed with a file and the sample was electropolished until shiny. It was then swaged, with one pass, into a

cylindrical rod 0.137 inches in diameter and electropolished again. The sample was sealed, while in He atmosphere, in a Ta tube which in turn was sealed in a glass tube. The protected sample was then placed in an annealing oven. Sample 1 was annealed for 10 hours at 250 C; then at 220 $\pm$ 6 C for 151 hours. Sample 2 was annealed at 250 C for 60 hours. Sample 3 was annealed for 190 hours at 250 C.

Unfortunately, sample 3 was partially damaged when it was being sealed into the Ta tube so this sample was somewhat shorter than the others. One end was melted and fused into the Ta in the process of welding the tube. Most (90%) of the sample appeared to be unaffected and the damaged portion was cut away. Spectrographic analysis showed no trace of Ta in the remaining piece.

The amount of unwanted rare earth magnetic impurities in the samples was below the detection limit of spectroscopic analysis. Sample 1 appeared to have a faint trace of chromium, although the measurement was obscured due to interference from another emission line. Sample 2 showed faint traces of nickel while sample 3 appeared free of contamination. Table 3 shows the complete listing of the results of qualitative analysis of the samples by emission spectroscopy.[1]

Another problem in sample preparation was the occurrence

---

[1]The analysis was performed by Analytical Services Group II, Ames Laboratory, Ames, Iowa.

Table 3. Emission spectroscopy results[a]

	Sample 1	Sample 2	Sample 3
Al			
Au			
Ca		FT	
Ce			
Co			
Cr	FTx		
Cu	T		
Dy			
Er			
Eu			
Fe	FT	FT	
Gd			
H			
Ho			
La	VS	VS	VS
Lu	M	W	W
Mg		FT-T	
Mn			
Nd			
Ni		FT	
Pr			
Sc			
Si		FT	
Sm			
Ta			
Tb		VW	W
Ti			
Tm			
Y			
Yb			

[a]List of symbols:
VS - very strong
S - strong
M - moderate
W - weak
VW - very weak
T - trace
FT - faint trace
d - element detected
- element not detected
x - interference.

of mixed phases of different crystal structure. In pure La the face centered cubic (fcc) structure is stable between the melting temperature, 910 C, and about 300 C and at lower temperatures the d-hcp modification is favored. The rapid cooling, which occurs after arc melting, allows some of the fcc to remain "frozen in" and considerable care is required to remove the fcc component. Neutron diffraction measurements were used to determine how much fcc was present in the "as cast" condition and how effective the annealing procedure was in obtaining the pure d-hcp structure. Table 4 shows the results of the neutron measurements.

Table 4. Neutron diffraction data on sample 1[a]

	d-hcp 102 peak $\|S\|^2 = 9f^2$	d-hcp 103 peak $\|S\|^2 = 3f^2$	fcc 200 peak $\|S\|^2 = 16f^2$
"as cast"			
C =	17,347	4338	1393
2 θ =	23.79	26.89	25.79
"annealed"			
C =	--	3042	288
2 θ =	--	26.88	25.95

[a]List of symbols: S - structure factor
f - scattering length
C - actual number of counts in peak
2 θ - scattering angle.

For these samples the preferred orientation of the crystals contributes only about a 5% error to the peak intensity so this factor is not important. If one combines the measured intensities of the peaks with the structure factor (50) one can estimate the amount of fcc material in the "as cast" condition to be 5.6% and the amount of fcc material in the annealed sample to be 1.6%.

A final step in sample analysis was to observe the grain structure visually, with 250x magnification, on a planar cross section parallel to and including the axis of the cylindrical sample. There was a noticeable decrease in grain size toward the outer edge of the sample, presumably due to preferential "cold working" in swaging the sample from square cross section to circular cross section of nearly equal area. A qualitative guess about grain size would be: sample 1--2 x 10^{-5} cm^2, sample 2--3 x 10^{-6} cm^2, sample 3--1 x 10^{-5} cm^2. Sample 2 showed much heavier "faulting" compared with samples 1 and 3.

Equipment

Thermal conductivity measurements were made using a standard He-3 refrigerator shown on Figure 2. Operation of the refrigerator has been discussed by Taconis (51) so all details will not be given here. Temperatures above 1.3 K were obtained by admitting 5 or 6 mm of He-3 gas to the He-3

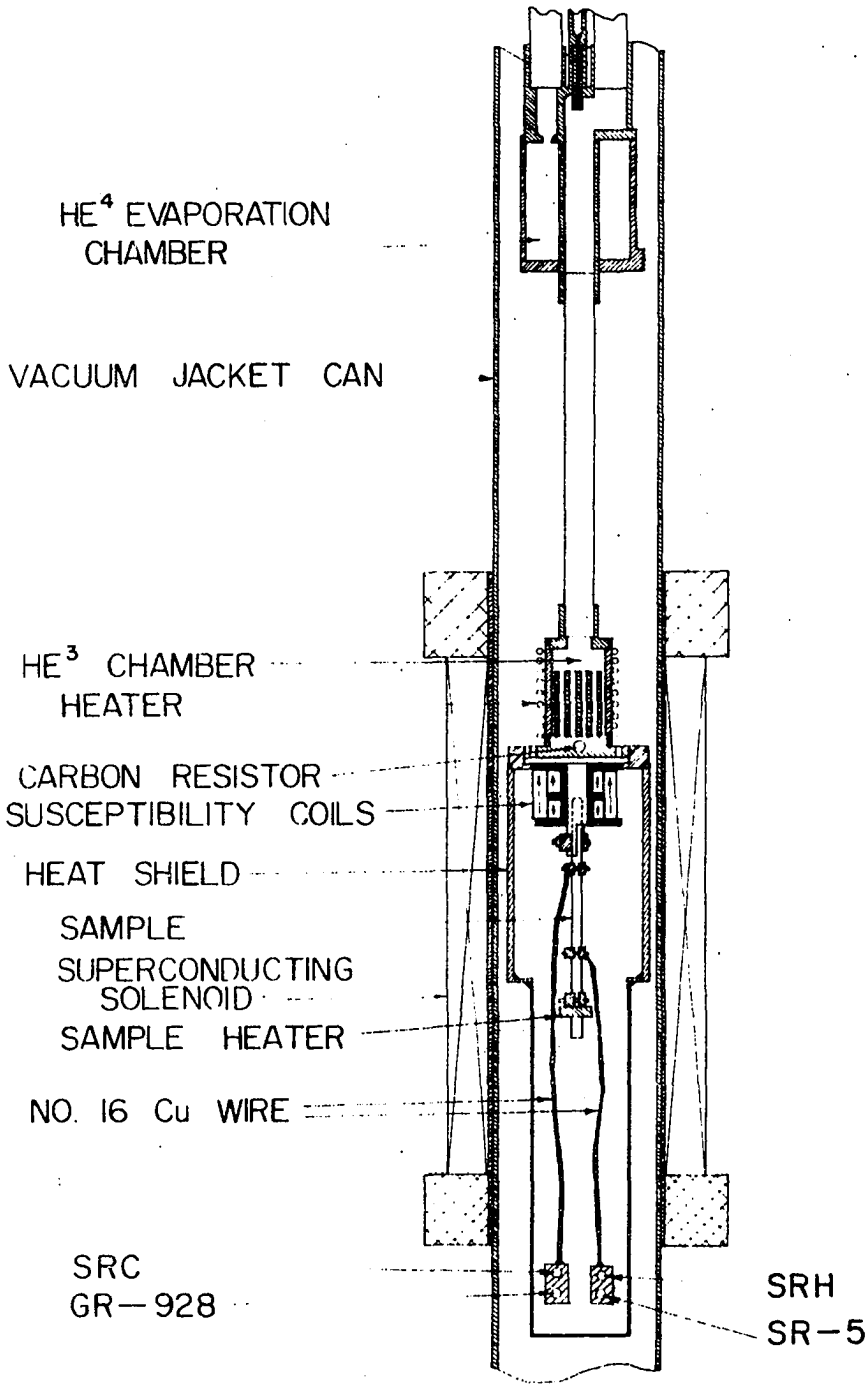

Figure 2. Thermal conductivity apparatus.

system to thermally link the He-3 chamber and He-4 chamber. Pumping through a manostat brought the He-4 chamber to the desired temperature. Below 1.3 K, temperatures were most easily maintained by first condensing about 1.3 cm^3 of He-3 and then pumping on it at a rate controlled by a sequence of valves. At all temperatures the most sensitive control of He-3 chamber temperature was obtained by changing the power to the He-3 chamber from a 1.2 kΩ manganin heater which was glued in place with GE-7031 varnish. The voltage drop across a carbon temperature sensing resistor, on the He-3 chamber, was measured with a Leeds and Northrup K-3 potentiometer. The off balance signal was amplified with a Keithley 153 microvoltmeter, and sent to a Bristol strip chart recorder where a retransmitting slidewire was used as a voltage divider to increase or decrease the heater current as the He-3 chamber became colder or warmer. A critical factor in obtaining good stability above 1 K was the amount of He-3 exchange gas. Too little would provide insufficient cooling power and the sample would warm. This was an especially serious problem while taking a thermal conductivity point since the sample heater was generating a few tenths of a mW, which then had to be conducted to the He-4 chamber via the exchange gas. Too much exchange gas (about 5 Torr or more) set up large temperature oscillations, presumably due to strong convection currents and refluxing in the exchange

gas. Problems due to drifting thermal emfs were eliminated by using rather large currents (on the order of 15 or 20 x 10^{-6} A) in the sensing resistor. When the regulating system was adjusted properly and equilibrium was reached, it was possible to establish constant temperature for periods of thirty minutes or longer within the following limits: 10^{-4} K at 5 K, 4 x 10^{-5} K at 2 K, and 5 x 10^{-6} K at 0.3 K.

The temperature dependent susceptibility of each sample was measured with a modified Hartshorn bridge shown on Figure 3. This 32 Hz bridge could typically resolve a superconducting transition to a few parts in 10^4 with a measuring field of 0.4 Oe. The sample coils (Figure 2) were wound with about 1500 turns of No. 38 copper wire on the primary and 3500 turns of No. 40 copper wire on each half of the astatic secondary. At 4.2 K the primary had a dc resistance of 50Ω, self inductance 168 mH, and a Q of 2.2. The corresponding quantities for the secondary were 17Ω, 128 mH, and 1.45. These numbers include lead effects.

A key system in the experiment was a modified 32 Hz Wheatstone bridge shown on Figure 4 which was used to measure carbon resistor secondary thermometers. The bridge is arranged so that the Speer carbon resistor at the cold end, (SRC), the Speer carbon resistor at the hot end, (SRH), or the difference, (SRC-SRH), could be sequentially measured

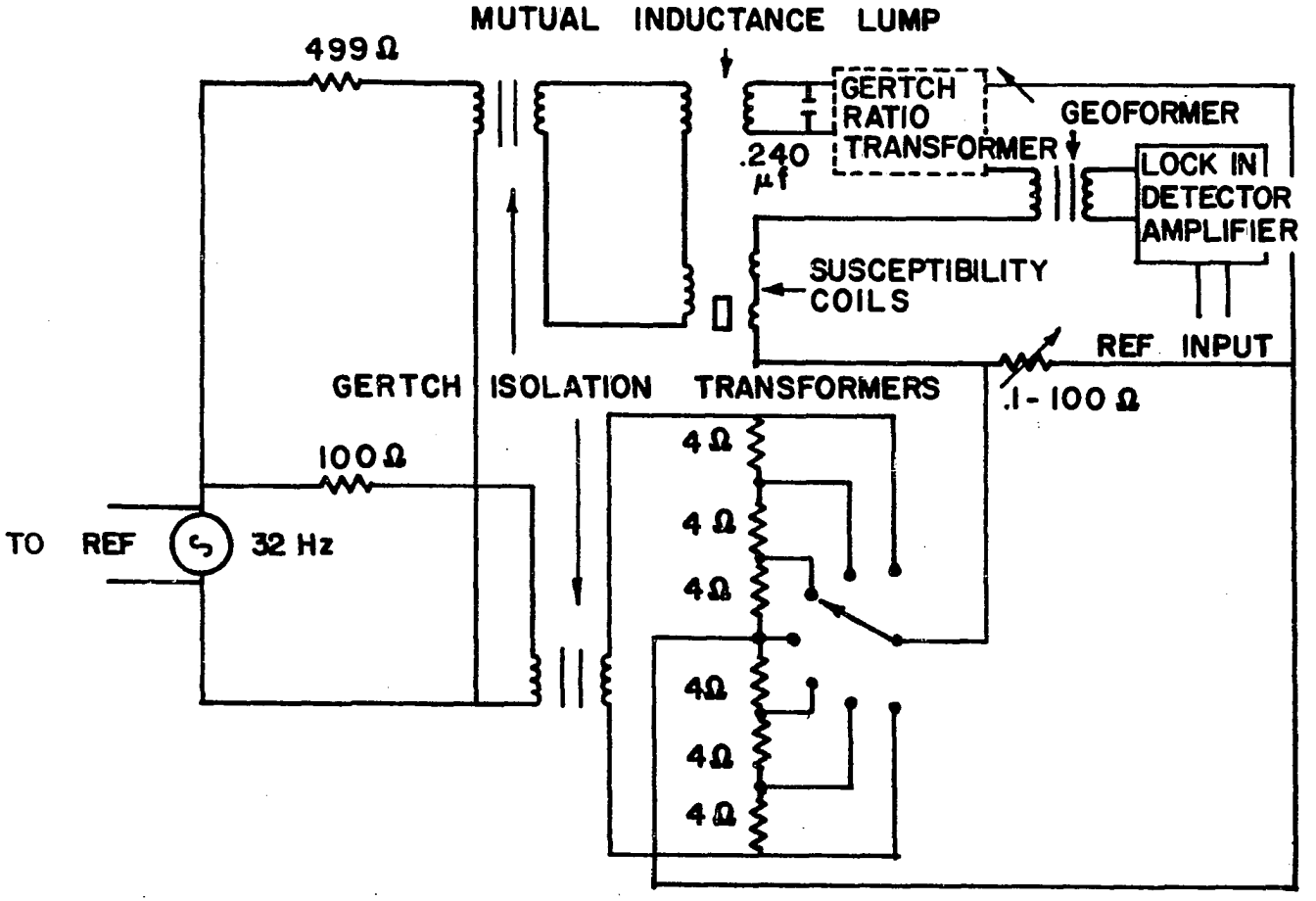

Figure 3. Mutual inductance bridge.

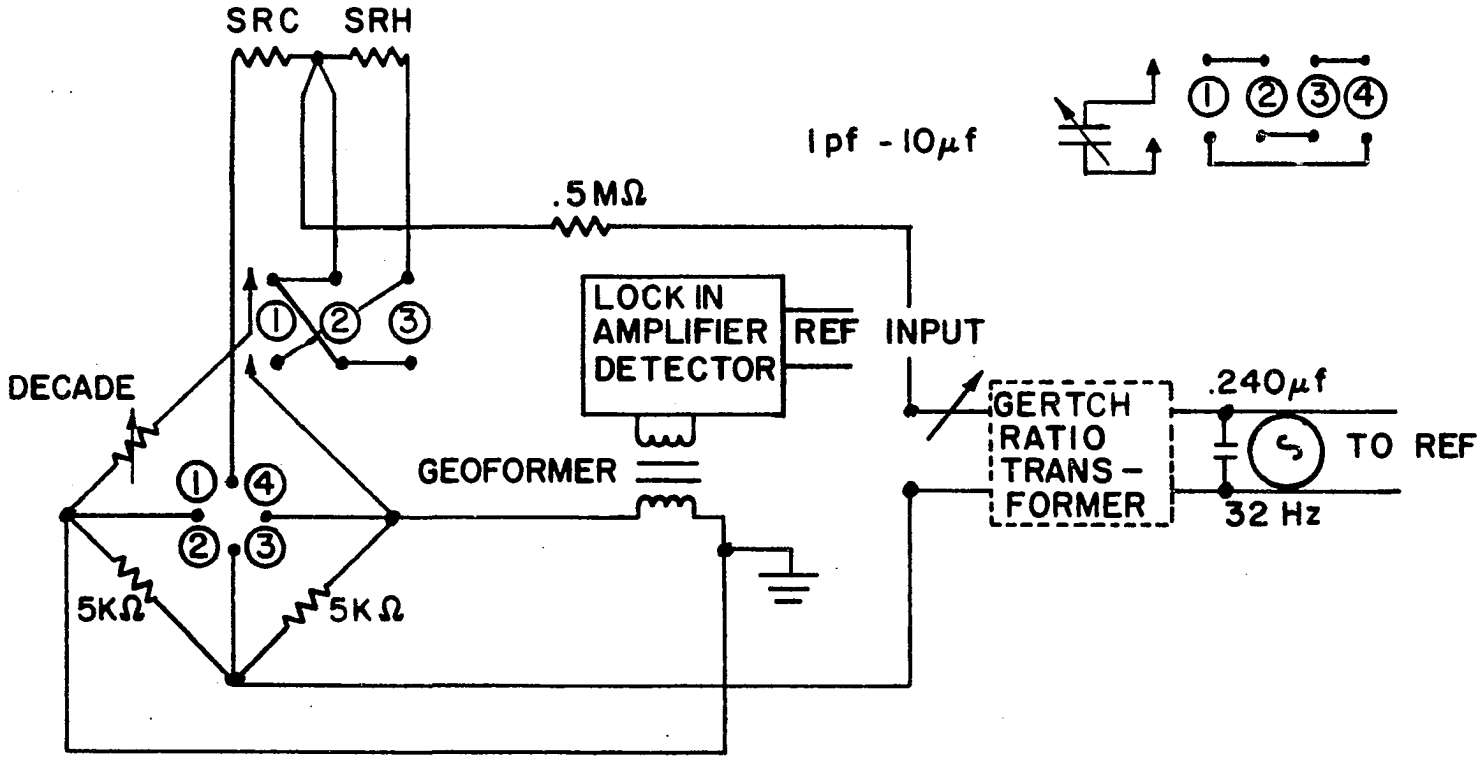

Figure 4. 32 Hz Wheatstone bridge.

by turning a switch.[1] The differential measurement is especially important since the factor limiting precision in measuring thermal conductivity is the measurement of ΔT which in turn depends on ΔR = SRC-SRH and not on the absolute values of SRC and SRH. The difference measurement reduces errors due to temperature drift in the two resistors and it also allows cancellation of residual magnetoresistance effects which remain even though the resistors are placed out of the main field (this point is discussed in further detail later). A three wire (or lead compensated) configuration is employed in each of the three measuring positions. The accuracy of the compensation was tested by substituting a series of precision resistors for SRC and SRH. This also indicated the presence of ground loops as well as uncompensated stray capacitive and inductive couplings. These problems were eliminated and the bridge was tested to be accurate to 0.05% over the resistance range of interest (1000Ω to 8000Ω). At 1000Ω the bridge could detect changes in resistance of 0.7Ω at a power level of 10^{-13} W. This amounts to a resolution capability of 7×10^{-9} V. Thermal conductivity measurements were made with a constant current of 2×10^{-6} A

---

[1]The resistors were the most closely matched of a group of twelve 1/2 watt Grade 1002 470Ω fixed composition resistors supplied by Airco Speer Electronic Components. For further details on their use as thermometers see Black, Roach, and Wheatley (52).

which implies power levels of from 0.5 to 4 x 10^{-9} W. With this current a resistance change of 0.01Ω could be observed.

A Guildline type 9180-B potentiometer along with a Guildline type 5214/9460 photocell galvanometer amplifier was used to measure the voltage and current in GR-928 (a germanium resistor previously calibrated by W. Decker), and in the sample heater. On a clear day it was possible to resolve 10^{-8} V at resistances below about 500Ω. Thunderstorms and other mechanisms for producing high voltage discharges adversely affected the null detector.

The sample heater power supply and the current supply for GR-928 used ten Hg cells in series along with a group of limiting resistors and switches. Both were stable to a few parts in 10^5 over half-hour periods.

An axial profile of the magnetic field produced by a Model X-4122 Varian superconducting solenoid is shown in Figure 5. It produced a 15 kOe field at 22.4 A. The current was supplied by a Spectromagnetic current regulated power supply with a stability of $\pm$ 10^{-5} over an eight hour period. Current in the solenoid was determined by potentiometrically measuring the voltage drop across a 0.01Ω Rubicon series resistor. After the desired field was reached the solenoid was switched into the persistent current mode and the power supply was turned off. There was no evidence of field decay in the persistent current mode.

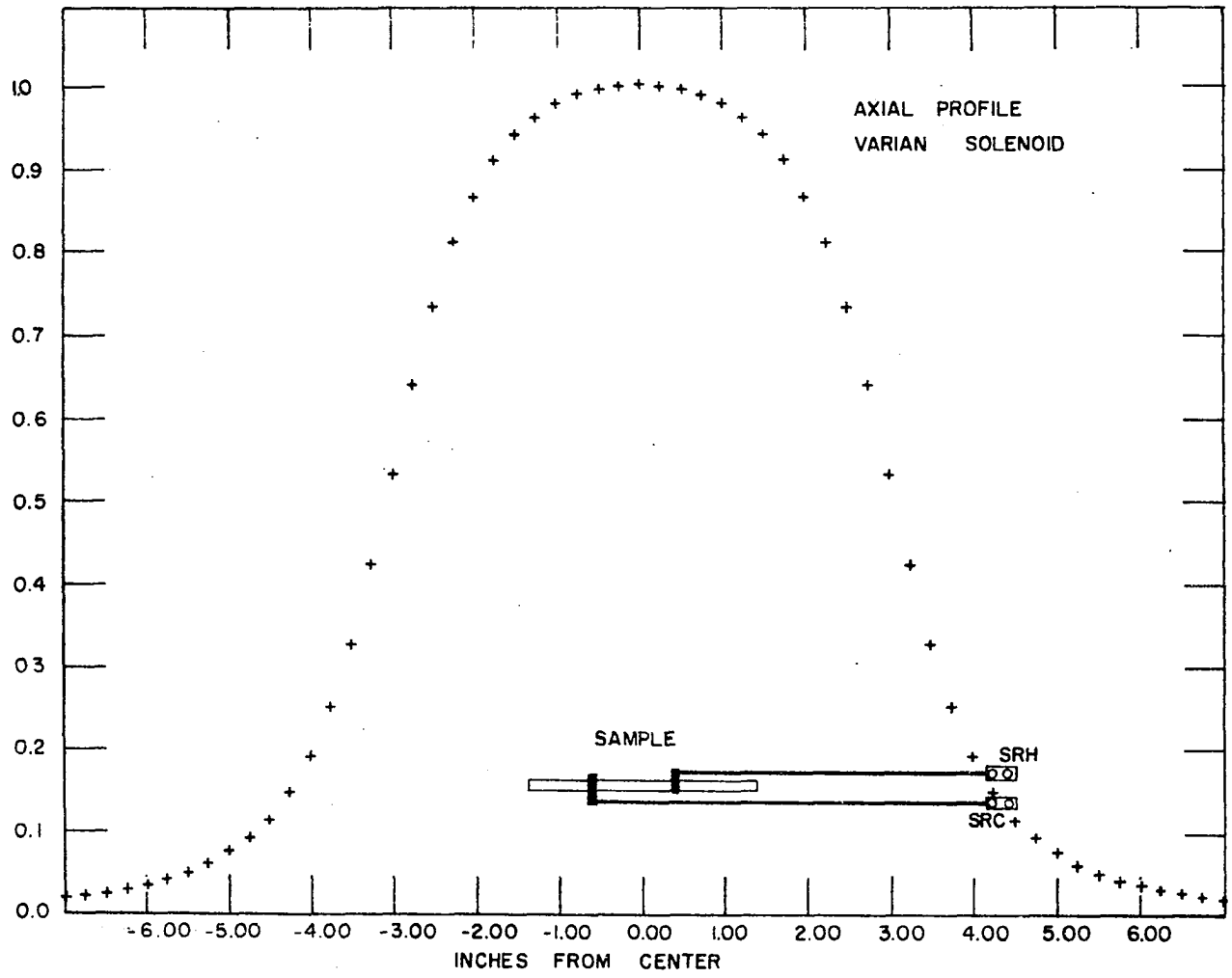

Figure 5. Calculated dependence of axial magnetic field of Varian superconducting solenoid.

Thermometry

The most important prerequisite for these measurements is an accurate temperature scale. A germanium resistor (GR-928) which was used as a secondary thermometer, had been previously calibrated by W. Decker (17) against the susceptibility of cerous-magnesium-nitrate (CMN) below about 1.5 K. Forty-eight additional calibration points were taken against the vapor pressure of He-4 for GR-928 from 1.5 K to 4.2 K to form a complete set of data from 0.3 to 4.2 K. These R vs T values were then fit to an equation of the form

$$\ln T_{calc} = \sum_{N} Q(N)(\ln R)^{N-1} \qquad (1)$$

by minimizing the root mean square deviation (rms dev), where rms dev is given by

$$(\text{rms dev})^2 = [\sum_{N} (T_N - T_{calc})^2]/(\text{NPTS}-1) \quad .$$

The criterion for a good fit reported by Rogers et al. (53) was used. The points to consider are that $(T - T_{calc})$ should be small for each point and $(dR/dT)_{calc}$ and $(d^2R/dT^2)_{calc}$ should be smooth and independent of the order of the fit. This insures that oscillations which are the result of "overfitting" do not occur. Temperatures were then generated with Equation 1 to compare with 3 separate sets of vapor pressure data obtained at different times over a two

year period. There was agreement to within 0.003 K for all points. The final fit was improved by dividing the data into two overlapping regions. The fit constants above and below 1 K are tabulated along with the data in Appendix A.

A possible source of error in the thermometry arises from the magnetoresistance of SRC and SRH. To obtain an estimate of the magnitude of this effect, the temperature was held constant by maintaining a constant vapor pressure over the He-4 space and the magnetic field dependence of the resistors was measured. An applied field of 11 kOe was required to drive sample 1 normal and fields of less than 2 kOe were required for samples 2 and 3 so these are the fields at which we need to know the magnetoresistance. If no correction were made for magnetoresistance an 11 kOe field would cause an error in T of 0.1 K so it was decided to move the resistors out of the field on the end of long copper rods. The calculation displayed on Figure 5 shows that the field at SRC is 1.7 kOe if the field at the center is 11 kOe but the actual reduction in field is somewhat larger since the calculation is for a point on the axis and the resistors are off axis. Previous measurements at this laboratory[1] have shown carbon resistor SR-5 to be relatively

---

[1]D. K. Finnemore, Ames Laboratory A.E.C., Ames, Iowa. Magnetoresistance data. Private communication. 1968.

insensitive to the field in this region, although its high resistance at low temperatures makes it inconvenient to use as a thermometer. Hence, SR-5 was used to indicate constant temperature as the field was turned up to 11 kOe. The reduction in field was 90% compared to the calculated value of 85%. In this configuration the error is about 0.005 K at 4.1 K and smaller at lower temperatures. The magnetoresistance data of Black, Roach, and Wheatley (52) on Speer carbon resistors of the type used in this experiment indicate that a 1.7 kOe field at 0.3 K would cause a change in R of less than 0.3%, which results in a temperature error of less than 0.0007 K. The error cancels out in measurements of ΔT if both resistors have the same magnetoresistance. Another check on the importance of this error was the measurement of the normal state thermal conductivity (K_n), with the field at 0 and at 11 kOe. The values were the same within 0.5% for sample 1. This is comparable to the normal scatter in the data. With the field smaller by a factor of five in samples 2 and 3, the error becomes completely negligible.

Heat leaks

One of the complicating features of these measurements is that the conductivity of these samples changes by more than two orders of magnitude in the relevant temperature

range. To obtain sufficiently accurate high temperature data it was necessary to choose the area/length (A/l) ratio small enough to stay within the restrictions imposed by the limited cooling power of the refrigerator. This resulted in an abnormally high thermal resistance at low temperatures. Hence it was very important to keep the heat leak small. In this experiment the sources of heat leak were: 1) conduction from the He-3 chamber to the lower end of the sample via the nine wires to the heater, SRH, and SR-5, 2) ohmic heating in these wires, 3) ohmic heating in SRH and SR-5, 4) residual gas conduction, 5) radiation, and 6) vibration. All of the above problems will be most serious in the low temperature region (He-3 chamber about 0.3 K). To minimize these effects, all leads were first thermally anchored at 4.2 K in the He-4 bath, then at 1.0 K on the He-4 chamber, and finally at 0.3 K on the He-3 chamber. A choice must be made regarding the size and length of wires going from the He-3 chamber to the sample. A small area/length (A/l) ratio for these wires decreases the heat leak of conduction but increases the ohmic heating. The compromise chosen was 15 cm of No. 44 manganin for all leads except the sample heater leads which were 30 cm of No. 36 manganin. The connection between SRC and SRH, which is required by the lead compensated bridge circuit, is 16 cm of No. 36 manganin. Anderson et al. (54) give the thermal conductivity for manganin as (0.555 T) mW/K-cm and

the corresponding resistivity, obtained from the Wiedemann-Franz law, is 44.1 $\mu\Omega$-cm. Assuming a maximum ΔT of about 0.3 K, the total heat conducted to the bottom of the sample is less than 10^{-8} W. This includes ohmic heating in all the leads except the heater current leads. This error goes as the ratio of lead resistance to heater resistance which is about 1/2%. A first order correction was obtained by attaching one heater voltage lead next to the heater and the other next to the thermal anchor point on the He-3 chamber (55). This reduces the error to a few parts in 10^4. The ohmic heating in SRH was less than 20×10^{-9} W. SR-5 was not used during conductivity measurements. The pressure in the vacuum can, as measured by a Phillips Ionization Gauge at room temperature and three feet above the can, was always lower than 10^{-5} mm of Hg. Light traps prevented most of the room temperature radiation from reaching the can. The remaining radiation and residual gas conduction effects were further reduced with a heat shield in thermal contact with the He-3 chamber. Vibration effects were not important since care was taken to isolate pumps and the system was mechanically strong. A typical heat leak to the He-3 chamber from all sources was about 1 μW at 0.3 K. The He-4 chamber received 3 or 4 mW at 1 K. If the heat shield was not touching the vacuum can and no unexpected sources of heat were present, the apparatus would reach an ultimate low

temperature for that run between 0.28 K and 0.30 K.

As a final precaution the heat leak to the sample at 0.3 K was experimentally measured at the start of each thermal conductivity run by measuring the change in temperature of the ends of the sample when it was driven from the superconducting to normal states. The heat leak, $\dot{Q}_{HL}$, is given by

$$\dot{Q}_{HL} = \frac{K_s \frac{A}{l}(\Delta T_s^o - \Delta T_n^o)}{1 - \frac{K_s}{K_n}}$$

where $(\Delta T_s^o - \Delta T_n^o)$ is the change in ΔT (measured with the sample heater power equal to zero) as the sample is driven normal. Typical values for $\dot{Q}_{HL}$ were about 70×10^{-9} W. For the host sample this heat leak had a fairly large effect (ΔT_s^o about 0.03 K) but in the alloys it was an order of magnitude smaller. Although any possible error arising from the heat leak was cancelled by the data taking procedure, it's presence contributed to the misfortune of obtaining conductivity data no lower than 0.45 K for sample 1. The power at this lowest temperature data point was adjusted to be about three times larger than the heat leak and because of the extremely small conductivity this resulted in a rather large ($\Delta T \sim T/2 \sim 0.16$ K) temperature difference across the sample and also a temperature difference of about 0.07 K

between SRC and the He-3 chamber. Again these effects are not important in the alloys because of their higher conductivity.

For other temperatures the power to the sample heater was usually adjusted to obtain values of $\Delta T/T$ about equal to 0.1 or 0.2 in the regions where K was approximately linear and $\Delta T/T$ about equal to 0.05 in regions where K showed more curvature.

Calibration and data analysis

The basic idea of the procedure for taking data and analyzing it is most easily discussed graphically with the aid of Figure 6. Part a indicates the situation when the calibration data is taken. The sample heater power, P_H, zero and the area under the curve between T_H^o and T_C^o is the heat leak, $\dot{Q}_{HL}$, which produces a temperature difference from the hot end of the sample to the cold end, $\Delta T^o = T_H^o - T_C^o$. Each calibration point included a measurement of GR^o-928, SRC^o, SRH^o, and $\Delta R^o = SRC^o - SRH^o$ (the superscript means $P_H = 0$). In part b of Figure 6 the cooling power of the He-3 chamber is increased and at the same time the sample heater power is turned on in such a way as to keep SRH^o (and therefore T_H^o) constant. A measurement of P_H and T_C^p (the superscript p indicates $P_H \neq 0$) along with the previous measurement of T_C^o is enough to determine KA/l without knowing the actual values of T_H^o and $\dot{Q}_{HL}$.

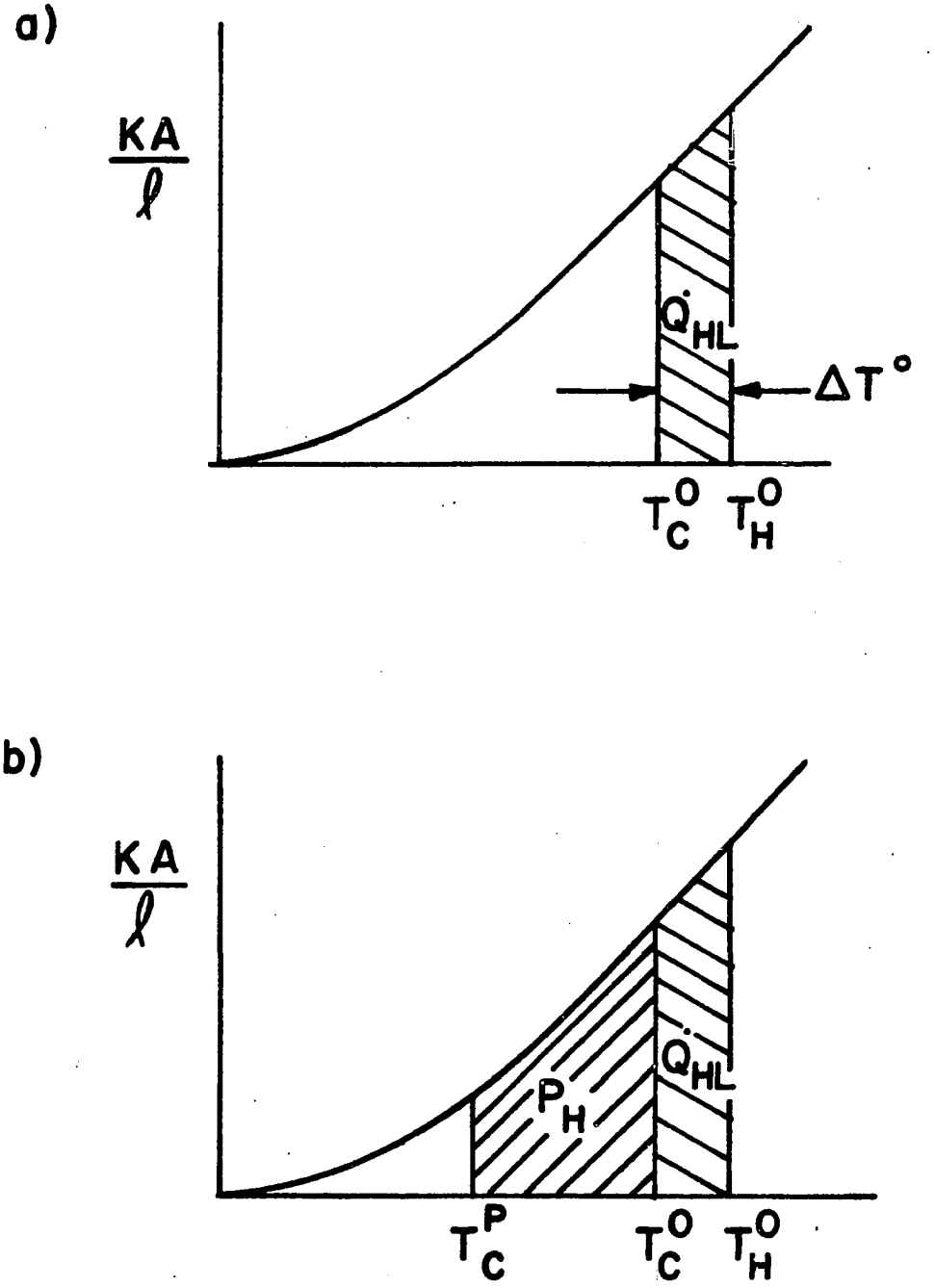

Figure 6. Illustrates heat leak cancellation procedure as explained in the text.

$$K\frac{A}{l} = \frac{P_H}{T_C^o - T_C^p} \qquad (2)$$

The first step in the measurement of any of these samples was to calibrate the Speer carbon resistor SRC against GR-928 and to determine ΔR^o as a function of SRC. Because SRC is mounted in the same copper block with GR-928, $\dot{Q}_{HL}$ should have no effect on the accuracy of T(SRC). Measurements of P_H, SRC^p, and ΔR^p were then obtained and analyzed with the calibration functions to obtain KA/l in a way entirely equivalent to the graphical explanation given above, provided $\dot{Q}_{HL}$ is the same during both measurements. During the conductivity measurements shifts in $\dot{Q}_{HL}$ could be easily monitored by observing shifts in ΔR^o.

An alternate way to take the data would have been to obtain ΔT from the two SRC measurements rather than from ΔR. However, through cancellation of the various errors the difference method (ΔR method) leads to data roughly 4 times more precise (23) than that obtained through separate calibration and measurement of SRC and SRH.

Geometry factors

The largest source of error in obtaining absolute values of K is the determination of A/l. The rather large collars (about 3 mm) introduce the question of effective length between SRC and SRH. Berman (56) has considered the problem

by making several sets of measurements on the same sample using different distances between collars and treating the effective length as an unknown. His result was that the distances between the midpoints of the collars can be used as l. Evidently the contact resistance between collar and sample is large enough to prevent much parallel heat flow and the collar takes up the average temperature of the section of the sample it is touching. Another problem Berman (57) considers is the failure of the simple formula (Equation 2) when the thermometer collars are close to the heat sink or to the heater. Under these conditions the temperature gradient is not uniform over the sample. His calculation shows that a spacing of a few mm, which was used in this experiment, eliminates problems of this sort.

The area of the sample was measured with a traveling microscope. Diameters were measured at 7 or 8 positions along the length of the sample and averaged. The error in area was mostly due to variation in area as a function of length. A cathetometer was used to measure the length in situ. Table 5 gives the results. The l/A ratios are probably no better than 2%.

Table 5. Geometry factors

	A, $10^{-3}cm^2$	l, cm	l/A, cm^{-1}
Sample 1	88.246 ± .440	3.424 ± .020	38.81 ± .43
Sample 2	93.21 ± .71	3.4515 ± .0240	37.03 ± .55
Sample 3	92.40 ± .50	3.570 ± .020	38.64 ± .43

Theory

For the materials discussed here, there are two important carriers of heat (the electrons and phonons) and six scattering mechanisms (the electrons, phonons, impurities and other point defects, dislocations, grain boundaries, and sample boundaries). A major difficulty then is to separate these various contributions so that one can discuss the electronic behavior. Ideally one would like to have samples in which electrons are the only carriers of heat and impurities are the dominant scattering mechanism because in this case the carrier velocity and mean free path are independent of temperature and the analysis of the data is fairly straightforward. For these La-Lu-Tb alloys the electronic heat transport, limited by impurity scattering, is a major contribution in the normal state but the presence of phonon

conduction, limited by electron scattering and other mechanisms, provides the major uncertainty in the results. Fortunately there are fairly detailed theories for these various contributions which have been used to give the proper temperature dependence for each term.

Most of these theories are based on a solution of the Boltzman transport equation with a relaxation time approximation. The following notation will be adopted in discussing the results of these calculations: A subscript e or g denotes whether the carriers are electrons (e) or phonons (g); the subscripts n or s denotes whether the sample is normal (n) or superconducting (s); these subscripts are separated by a slash from a subscript which indicates whether the scattering is due to electrons (e), phonons (g), point defects (p), dislocations (d), grain boundaries (b), or sample boundaries (l). For example normal state phonon conductivity limited by electron scattering would be denoted by $K_{gn/e}$. The letters A and B will denote the adjustable coefficients in the electronic and lattice conductivities respectively.

The normal state electronic conductivity limited by point defect impurity scattering is $K_{en/p} = AT$, where the Wiedemann-Franz law implies that A is the product of electrical conductivity (σ) and the Lorentz number (L). The normal state phonon conductivity limited by electron

scattering is given by $K_{gn/e} = B_e T^2$ (58). The Lindenfeld-Pennebaker (59) "universal curve" formalism allows for temperature dependencies other than T^2 for this term but the results for all three alloys in this experiment were not consistent with their analysis so the simpler T^2 dependence was assumed. The values of $K_{gs/e}$ and $K_{es/p}$ in the host material can be obtained from the Bardeen, Rickayzen, and Tewordt (BRT) (58) calculation of K_{es}/K_{en} and K_{gs}/K_{gn} (call the ratios R_e and R_g respectively). The calculation which is based on BCS theory is in good agreement with experiment when phonon conduction is negligible (60) and also when there is an appreciable phonon contribution (61, 62).

Klemens (63, 64) has given a detailed discussion of the dependence of the phonon conductivity on other scattering mechanisms and Slack (65) has listed his formulas in a very convenient form. We have repeated Slack's presentation below except that only the temperature dependence will be given and all the other factors have been gathered into one adjustable parameter

Sample boundary scattering : $K_{g/l} = B_l T^3$

Grain boundary scattering : $K_{g/b} = B_b T^3$

Dislocation scattering : $K_{g/d} = B_d T^2$

Point defect scattering : $K_{g/p} = (B_p T)^{-1}$.

The effects of more than one scattering mechanism are usually taken into account by assuming the thermal resistances are additive. This approximation is strictly valid only when all of the scattering mechanisms have the same phonon frequency dependence. There is experimental evidence (65, 66, 67, 68) that this approximation is invalid in some cases but it will nevertheless be used in the analysis of the phonon contribution.

Results and Discussion

Normal state data

Figures 7, 8, and 9 show that $K_n = AT + BT^2$ is a fairly good description of the normal state data. The constants A and B which were obtained by a least square fit of the data to this equation are given in Table 6. There appear to be

Table 6. Normal state parameters

	$\frac{A}{\frac{mW}{K^2\text{-cm}}}$	$\frac{B}{\frac{mW}{K^3\text{-cm}}}$	$\frac{R_{300}}{R_4}$	ρ_{300} $\mu\Omega$-cm	ρ_4 $\mu\Omega$-cm	$\frac{L_{W-\Omega}}{K^2} \times 10^8$
Sample 1	2.304	0.1148	6.737	67.23	9.979	2.30
Sample 2	3.034	0.1052	8.950	65.72	7.343	2.23
Sample 3	3.595	0.0865	9.324	59.58	6.390	2.30

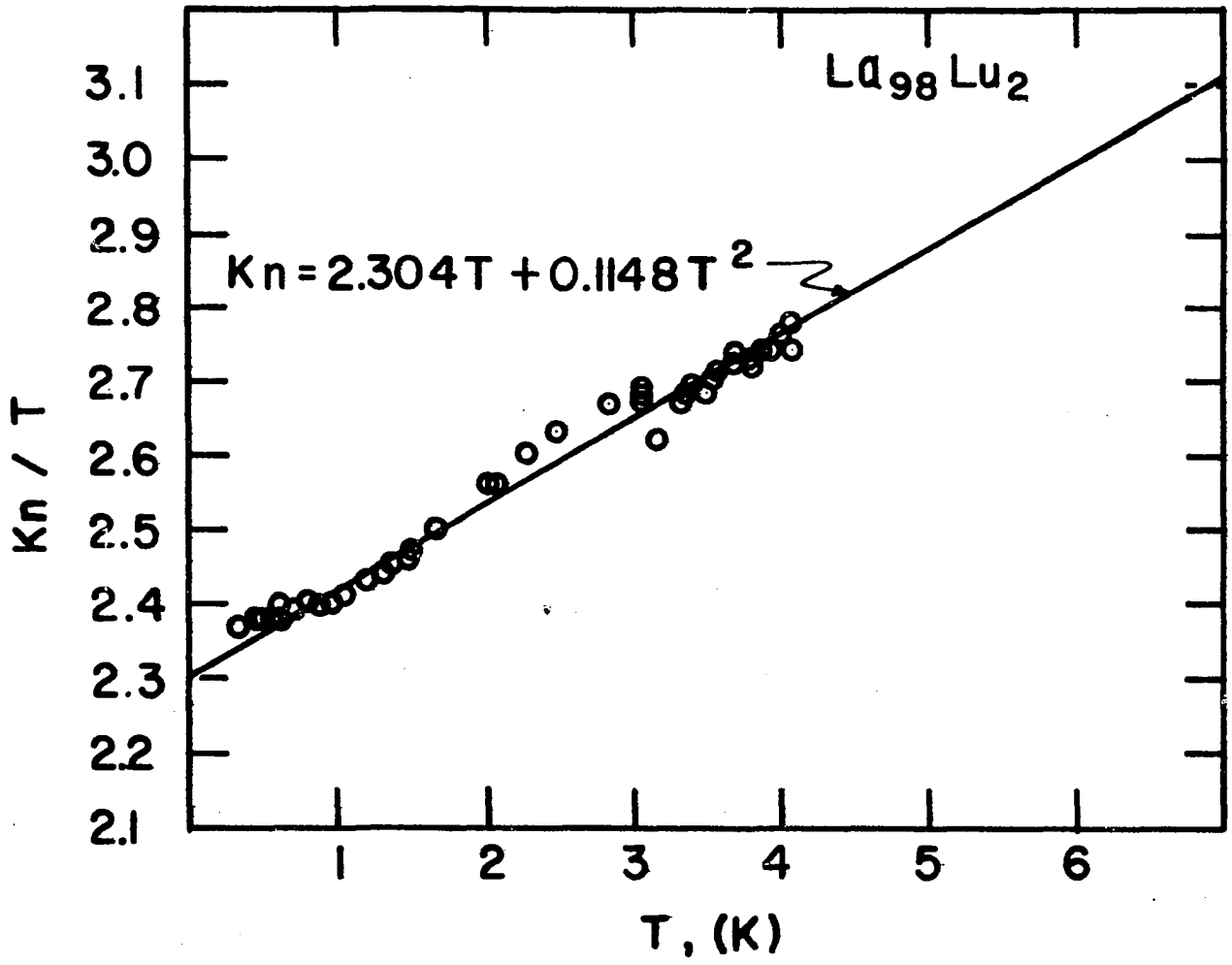

Figure 7. Normal state data for sample 1.

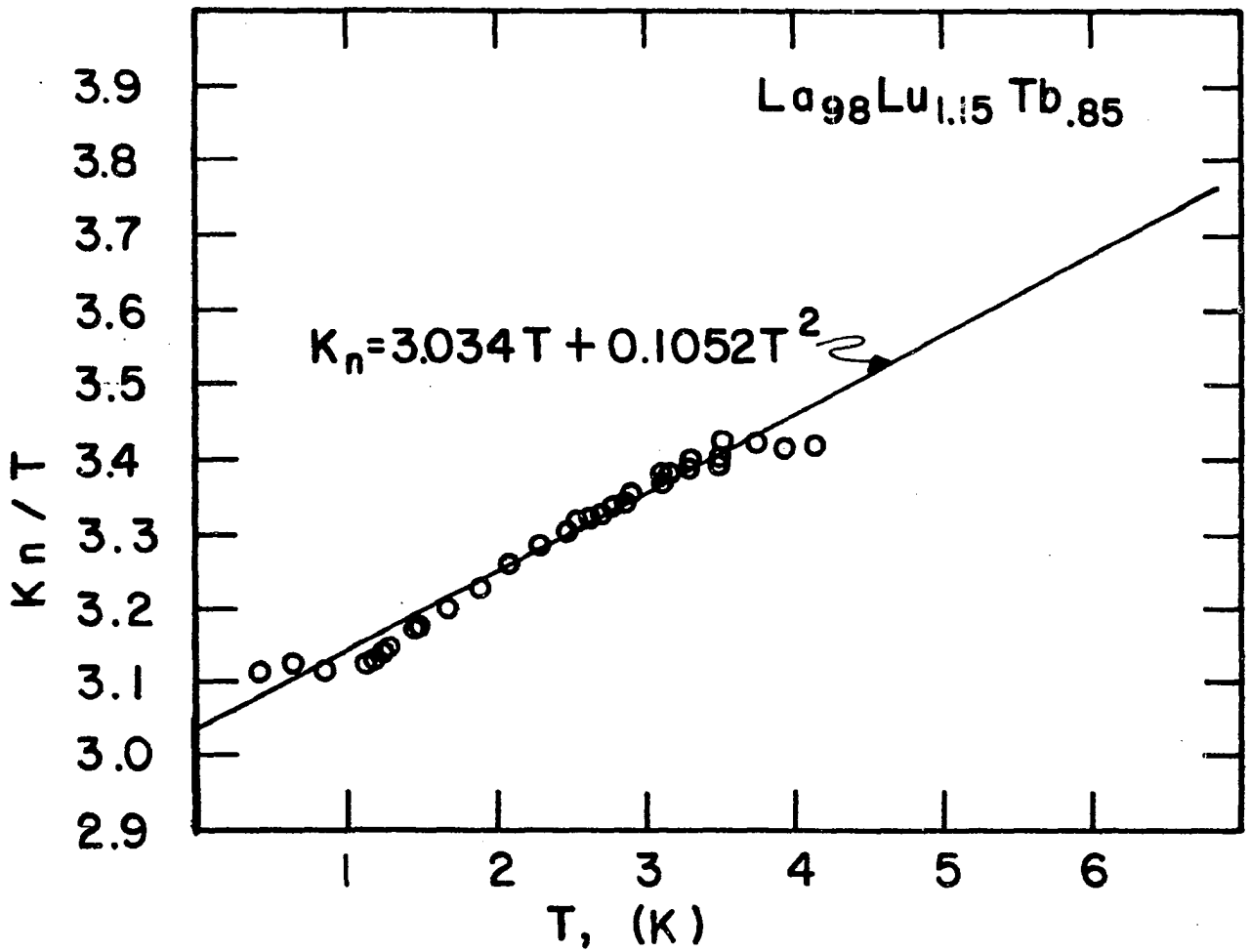

Figure 8. Normal state data for sample 2.

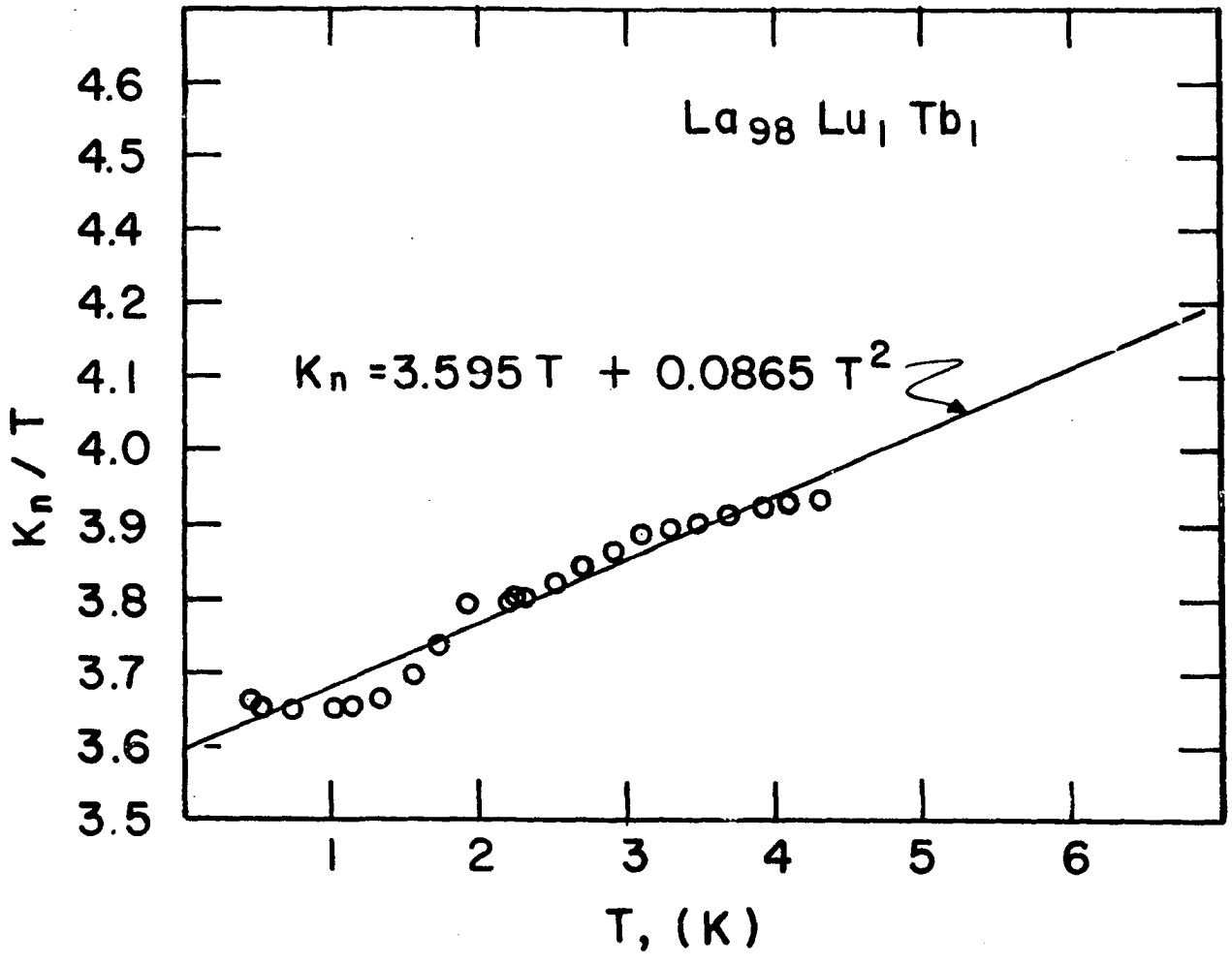

Figure 9. Normal state data for sample 3.

small systematic deviations from this equation which are probably due to small amounts of point defect and grain boundary scattering. An attempt has been made to separate these phonon contributions in a later section. However, the rms deviation of the data from this $K_n = AT + BT^2$ curve, for all three samples, is about 3/4% which is nearly the size of the scatter in the data.

The accuracy of the above separation of thermal conductivity into electronic and phonon contributions can be tested by obtaining the Lorentz number (L), which should be nearly the same for all three samples. The electrical resistivity at 4 K (ρ_4) was obtained from the resistivity ratio

$$\left(\frac{R_{300}}{R_4}\right)$$

and the room temperature resistivity (ρ_{300}) which was measured with a four probe method. Razor blades were used as the voltage probes and the A/l ratio was measured using techniques previously described. Table 6 lists these parameters along with the Lorentz number (L) which is obtained from the Wiedemann-Franz law. The experimental error in L is estimated to be about 5% resulting mainly from errors in the geometry factors. Within this limit all samples have the same Lorentz number which is about 6% lower than the free electron value which is $2.45 \times 10^{-8} \frac{W\text{-}\Omega}{K^2}$. This is a

very encouraging sign that there are no gross errors in the separation of the normal state electronic and phonon terms.

In the early stages of this work it was hoped that the normal state conductivities of the three samples would be nearly the same in that the total number of impurity atoms (Lu plus Tb) was held fixed at 2%. This is not the case. The electronic conductivity increases and the phonon conductivity decreases as Lu atoms are replaced by Tb atoms. Presumably Lu impurity atoms in a La host have a much higher scattering cross section for electrons and hence the increase in electronic conductivity as Tb is added. This effect of increasing electron mean free paths with decreasing Lu also accounts for the decrease in the phonon contribution. A complete explanation of this effect is rather complicated and the arguments are given in detail by Lindenfeld (59) and Pippard (69). In essence, however, this theory says that the mean free paths of phonons in both longitudinal and transverse modes decrease with increasing electron mean free paths. Hence the decrease in the phonon contribution in the alloys with smaller amounts of Lu.

In view of the above explanation sample 2 appears somewhat anomalous in that A is smaller and B and ρ are larger than expected. This effect probably arises from the annealing procedure since sample 2 was annealed for a substantially shorter time. An optical study of the samples showed that

it had far more twinning and smaller grain size and hence the grain boundary and dislocation scattering are greater and the phonon conductivity is correspondingly smaller.

Host phonon conductivity

A more detailed analysis of the phonon conductivity (or resistivity) into contributions from point defect, grain boundary, dislocation, and electron scattering is very difficult because there are so many adjustable constants. In the analysis which follows several assumptions are made in order to evaluate these constants and any conclusions which are drawn must be subject to the reasonableness of these assumptions.

At the outset the electron conductivity is assumed to be limited entirely by impurity scattering so that $K_{en} = AT$. As was mentioned earlier this gives a Lorentz number close to the theoretical value so this assumption has some foundation. The phonon conductivity in the normal state is then taken to be $K_n - AT$.

To understand the phonon conductivity in the superconducting state it is necessary to realize that electrons dominate the phonon scattering process in the normal state. In the superconducting state, however, the effect of this scattering mechanism is decreasing rapidly so the details of the other mechanisms can be more easily evaluated. Stated another way, the phonon mean free path due to electron

scattering increases with decreasing temperature below T_c because some of the electrons have dropped into the superconducting ground state and are no longer available for scattering. This leads to an increase in the phonon conductivity over the normal state value and at lower temperatures other scattering mechanisms such as dislocation, point defect, and boundary scattering become important. For a BCS like superconductor, such as La_{98} Lu_2, the ratio of these two conductivities, $K_{gs/e}/K_{gn/e} = R_g$, is well understood from BRT theory, as previously discussed, and the effect of electron scattering can be calculated with some confidence. For the Tb alloys, however, the theory for this correction has not yet been developed.

The general approach used for this detailed analysis of phonon scattering was to first assume that the theory, where it is available, is correct. That is we assume that K_{es} was described correctly by BRT theory (using a reduced gap of 3.70 (70)). Then one can assign the difference between the theory and the total conductivity (K_s) to the phonons ($K_{gs} = K_s - \text{BRT } K_{es}$). The next step was to assume that the thermal resistivity due to electron scattering

$$(W_e = \frac{1}{B_e T^2 R_g})$$

was also accurately described by BRT and then to fit the remaining resistivity (call it $W_{limit} = \frac{1}{K_{gs}} - W_e$) with some

combination of the other three possible temperature dependencies previously described. Each additional scattering mechanism introduces one adjustable parameter. The rms deviation of the experimental K_s data from the calculated K_s points can then be considered a function of the adjustable parameters and the computer was used to obtain values of the parameters which would minimize the rms deviation for a particular choice of scattering mechanisms. The choice which gave the best fit included point defect scattering, dislocation scattering, and internal grain boundary scattering.

In order to determine how sensitive the fit is to each of the adjustable constants we have systematically varied these constants separately. Each of Figures 10, 11, and 12 show the effect of changing one parameter above and below the "best fit" value. There is a systematic deviation of the K_{gs} points from the "best fit" curve that is outside the range of experimental error. This discrepancy could arise from a failure of the resistive addition approximation but it seems more likely that the best fit curve does not reflect the actual physics of the phonon scattering mechanisms. The above procedure should probably be regarded as a way to "parameterize" the phonon conductivity. The scattering mechanisms mentioned are present in the normal state also and so the normal state data was reanalyzed

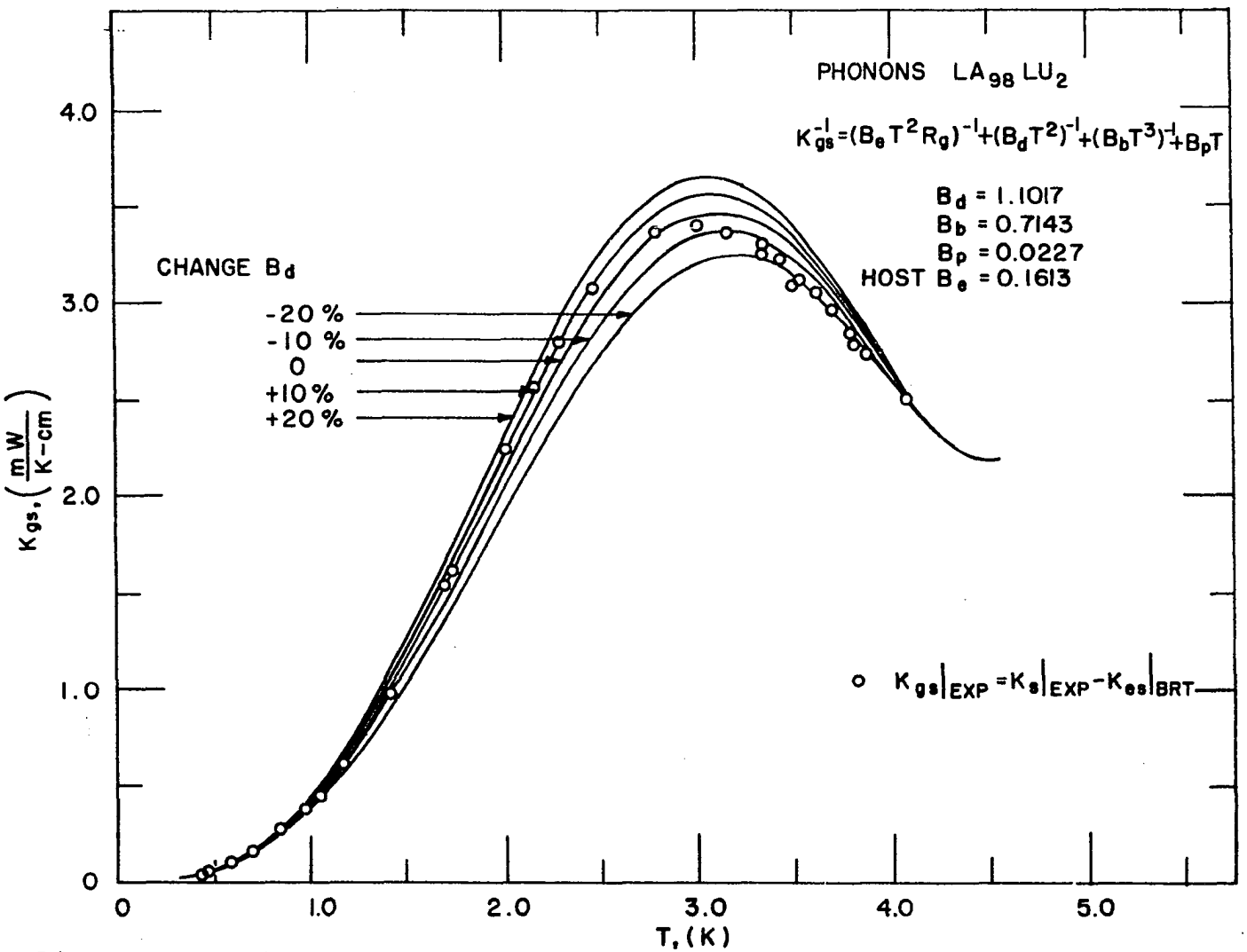

Figure 10. The circles are the values of K_{gs} obtained by subtracting the BRT values of K_{es} from the total experimental conductivity, K_s. The solid lines show the effect of changing the amount of dislocation scattering (Parameter B_d) from the "best fit" value.

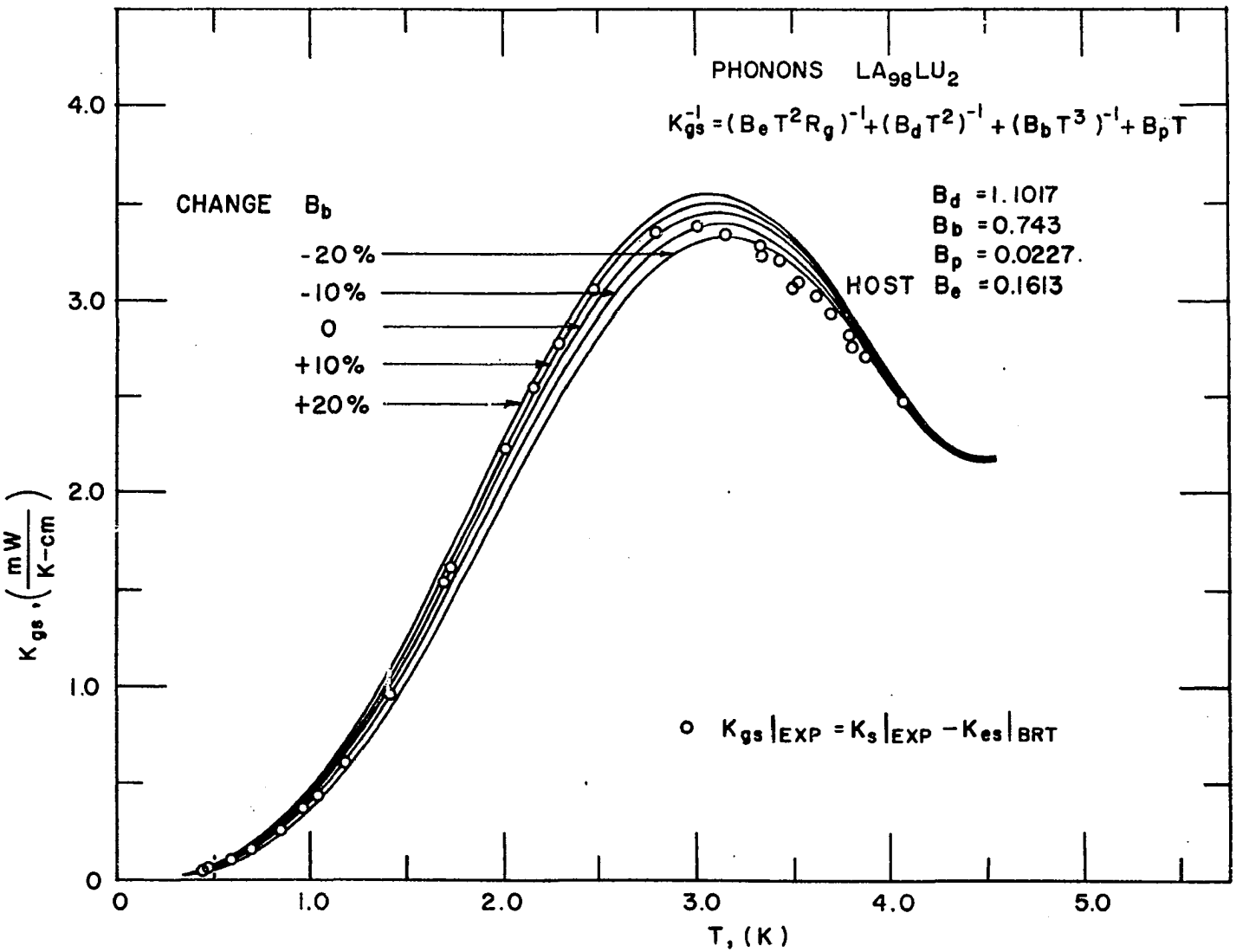

Figure 11. The solid lines show the effect of changing the amount of grain boundary scattering (parameter B_b) from the "best fit" value.

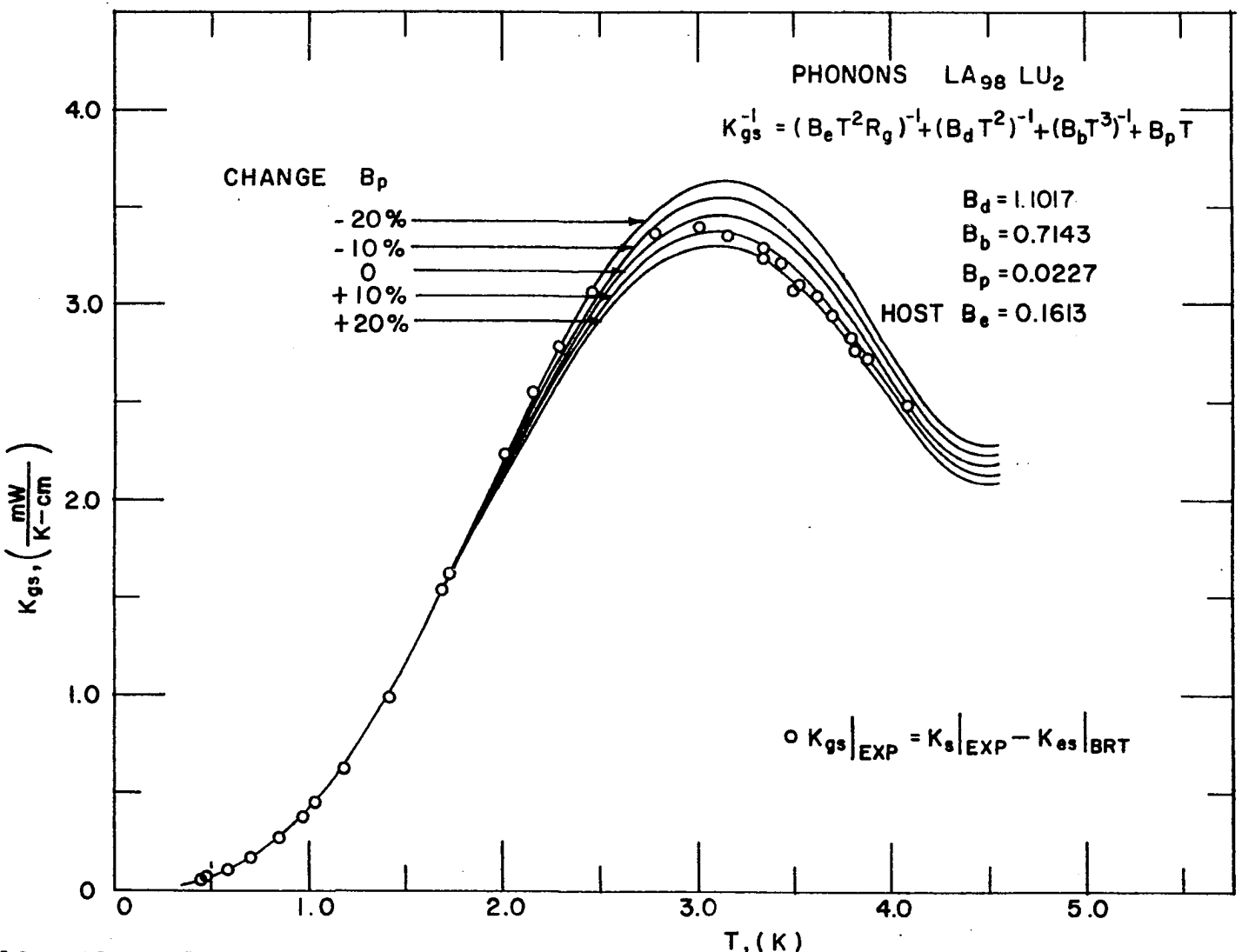

Figure 12. The solid lines show the effect of changing the amount of point defect scattering (parameter B_p) from the "best fit" value.

including the new terms and considering the coefficient A of the electronic conductivity and the coefficient B_e of the T^2 term to be adjustable parameters. The rms deviation of the new fit was about 0.1% better than the $AT + BT^2$ description and the new value of A agreed with the old value to within a few parts in 10^4. So that even if the analysis is not unique in selecting the phonon scattering mechanisms it is certainly consistent with all of the experimental data.

Figure 13 shows how successful the procedure was in obtaining agreement with the experimental values of K_s and K_n. A striking coincidence observed in La_{98} Lu_2 shown on Figure 13 was that K_{gs} was increasing (due to the R_g factor) below T_c just enough to compensate for the decrease in K_{es} so that the total conductivity did not appear to deviate from the normal state behavior until the temperature was about 1.5 K below T_c. That is, the increase in phonon conduction due to superconductivity can be as large or larger than the decrease in the electronic conductivity. Figure 14 shows these same results plotted in the form of the ratios, K_s/K_n and $(K_s-K_{gs})/(K_n-K_{gn})$.

Magnetic impurity alloys

The transition temperatures of the alloys as well as the host were measured by a differential susceptibility

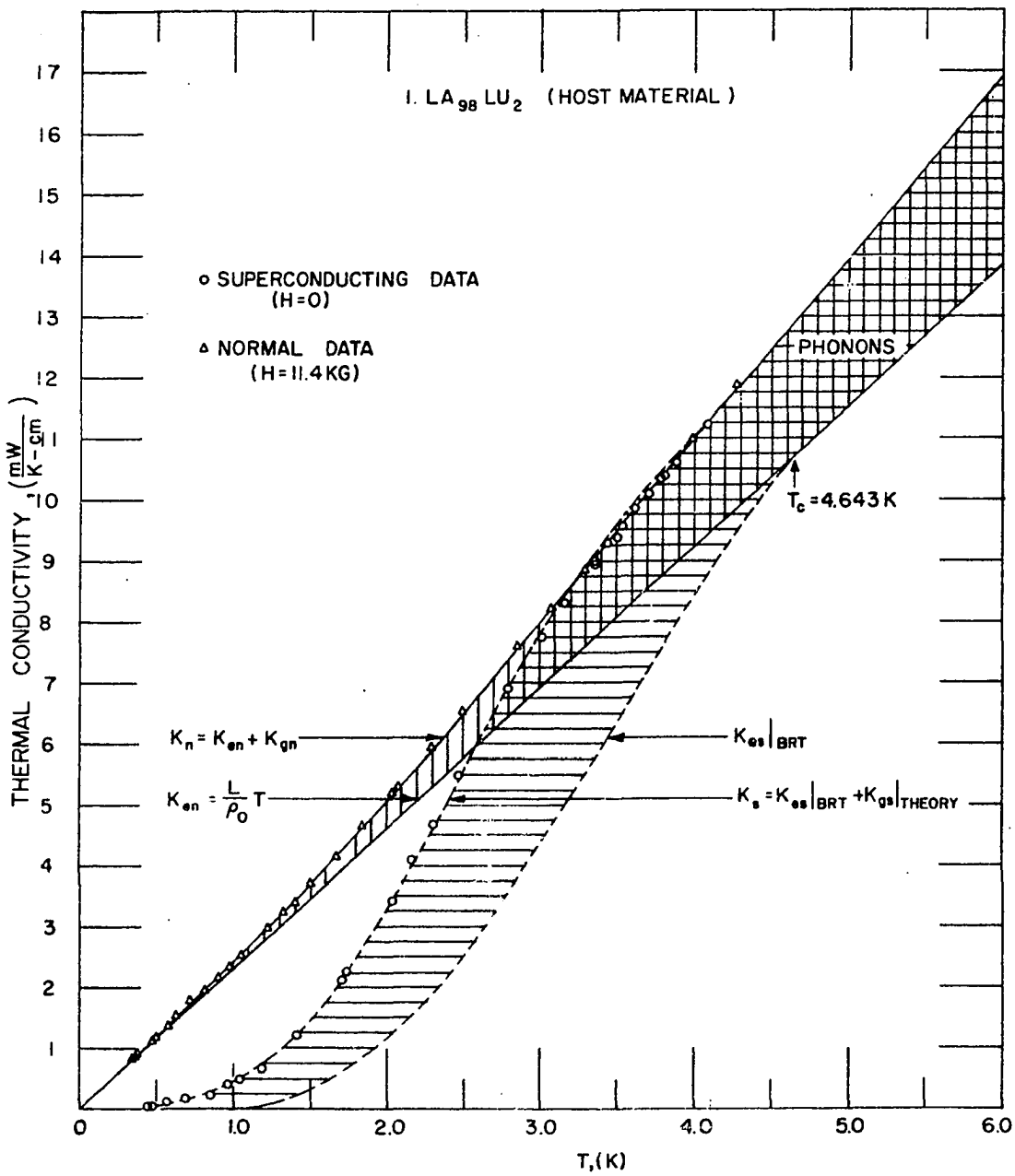

Figure 13. The normal state data are shown as triangles and the superconducting data as circles. The shaded area represents the phonon contribution to the total conductivity.

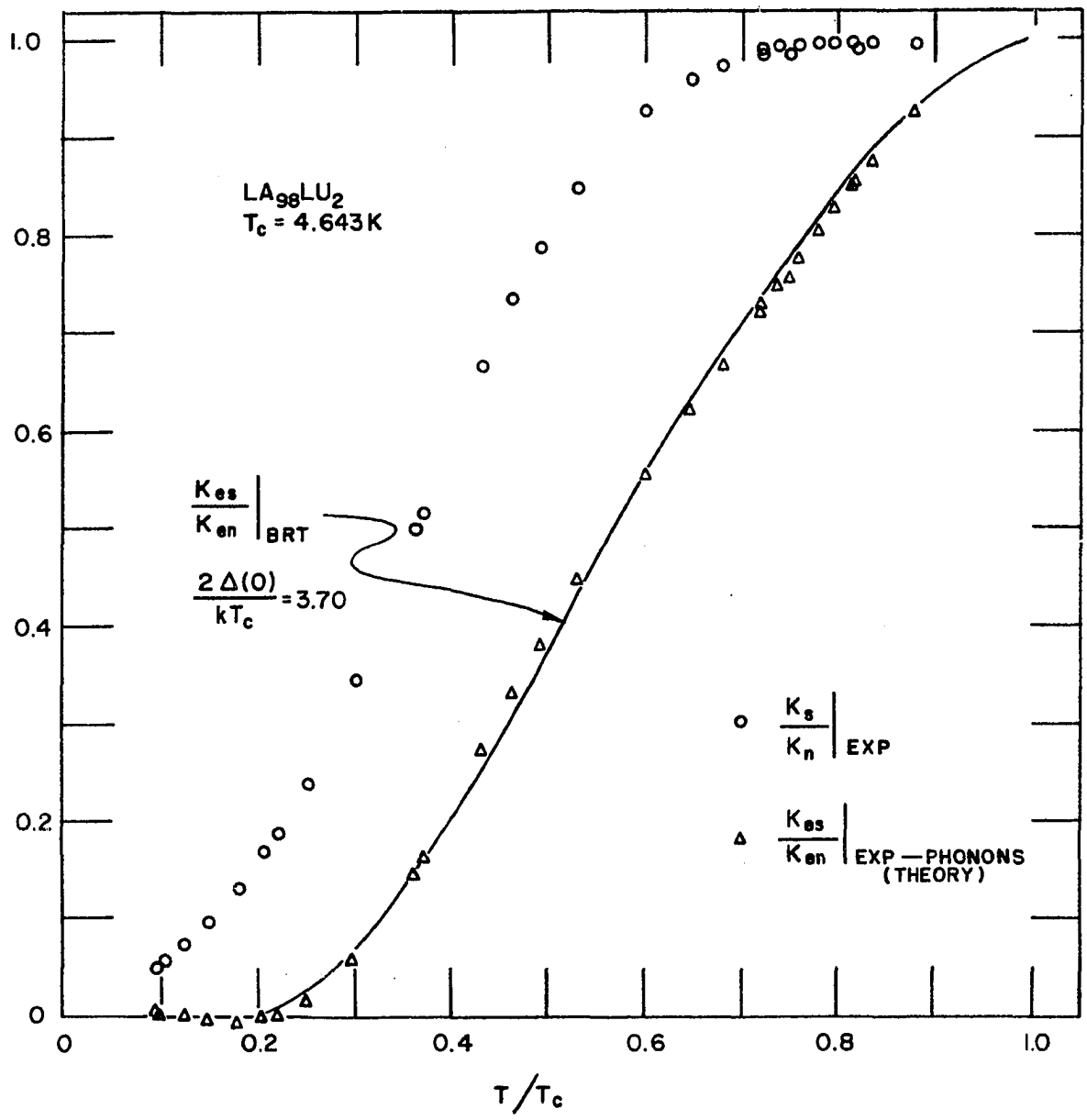

Figure 14. The ratios of total conductivity in superconducting state to that in the normal state are shown by the circles. The triangles show the result of subtracting out the phonon contribution.

technique. The midpoints of the susceptibility transition shown in Figures 15, 16, and 17 were defined as T_c. The transition of sample 2 is wider by a factor of two compared with samples 1 and 3. This is taken as further evidence for the importance of annealing as has been previously discussed. The dependence of T_c on the concentration of Tb, plotted in reduced coordinates, is shown in Figure 18. The value of n_{cr} is calculated from AG theory with the following equation,

$$\ln \frac{T_c}{T_{cp}} = \psi(1/2) - \psi(1/2 - 0.14 \frac{T_{cp}}{T_c} \frac{n}{n_{cr}}) \quad .$$

The transition of the two magnetic alloys lie somewhat above both the impurity spin correlation curve and the magnetic ordering curve also shown in Figure 18. The onset of impurity spin correlations is defined by the temperature at which the susceptibility shows deviations from paramagnetic behavior. Hence the excellent (better than 0.5%) agreement of these transition temperatures with AG theory is not surprising since the theory has been shown to be in good agreement for paramagnetic alloys. However Figure 18 also shows that samples 2 and 3 should enter the regions of impurity spin correlations below about 1.3 K and 1.5 K respectively. This is the region mapped out by the measurements of thermal conductivity shown on Figures 19 and 20. Bennemann (47) predicts an anomalous temperature dependence for the exchange

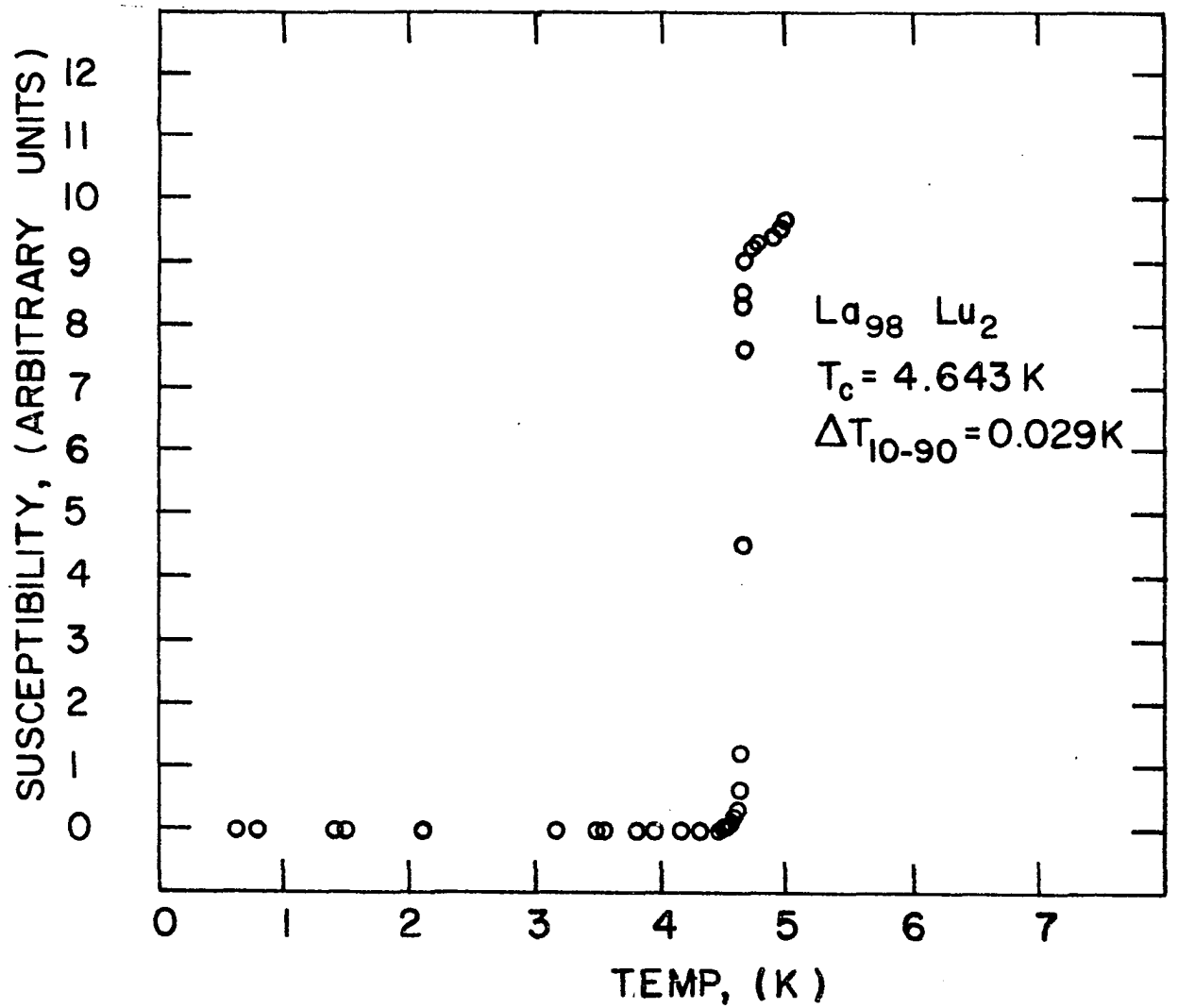

Figure 15. The susceptibility transition for the host sample. The extra structure above 5 K is probably due to the 1.6% of "frozen in " fcc structure.

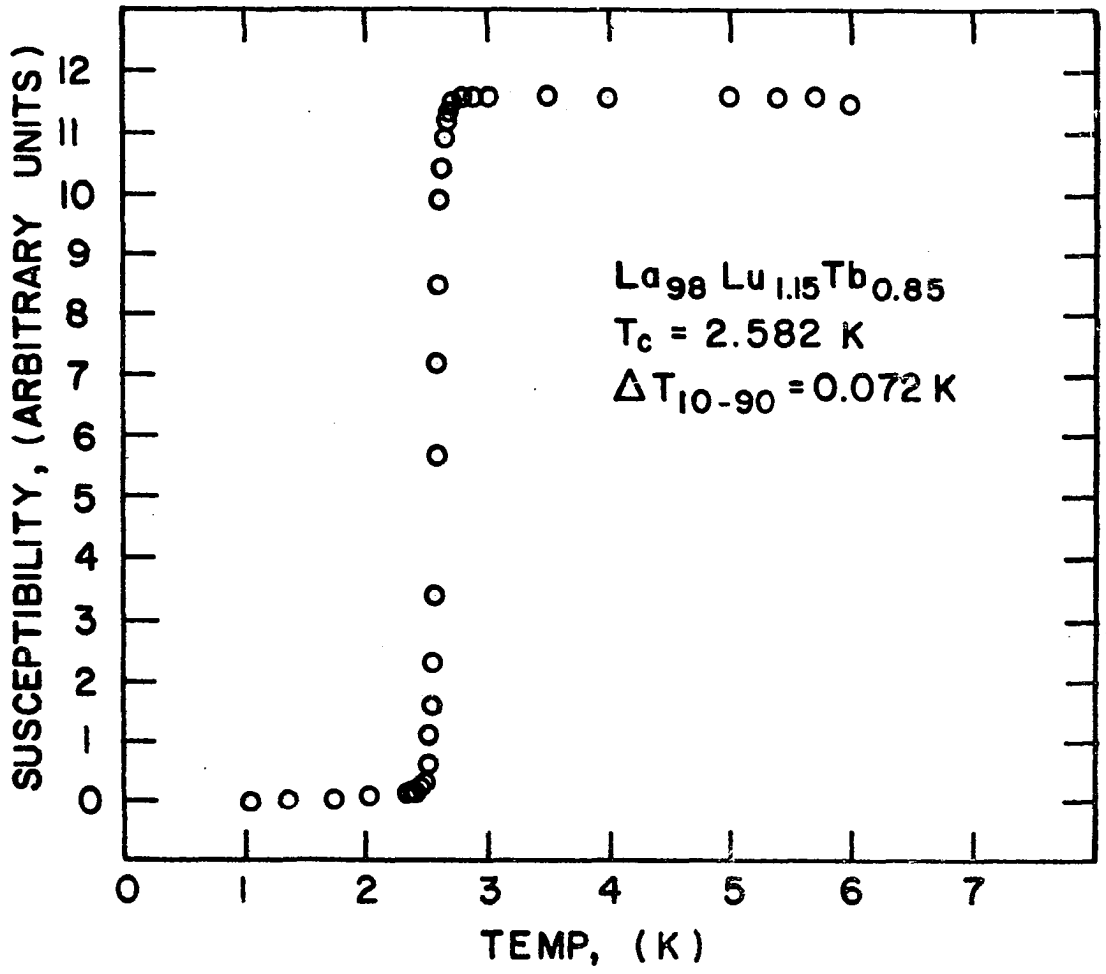

Figure 16. The susceptibility transition of sample 2.

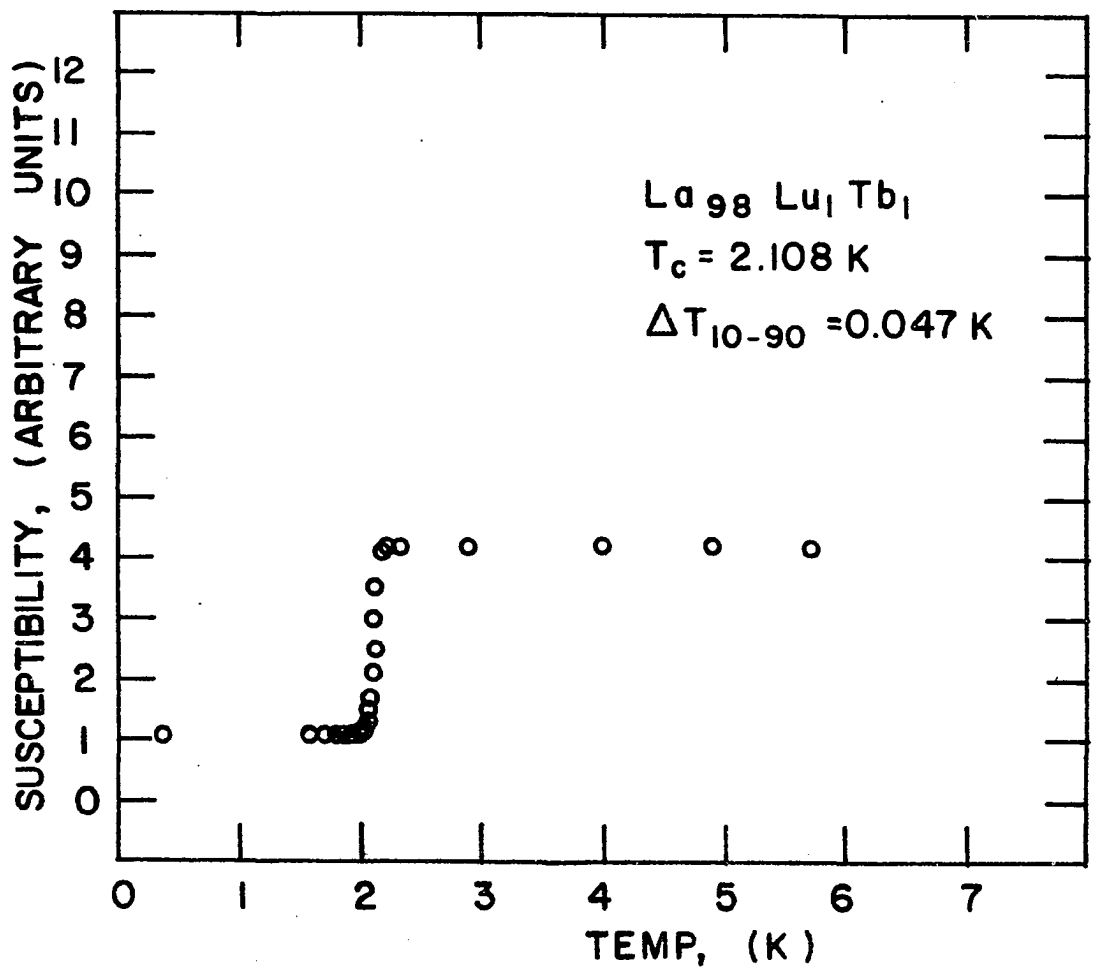

Figure 17. The susceptibility transition of sample 3.

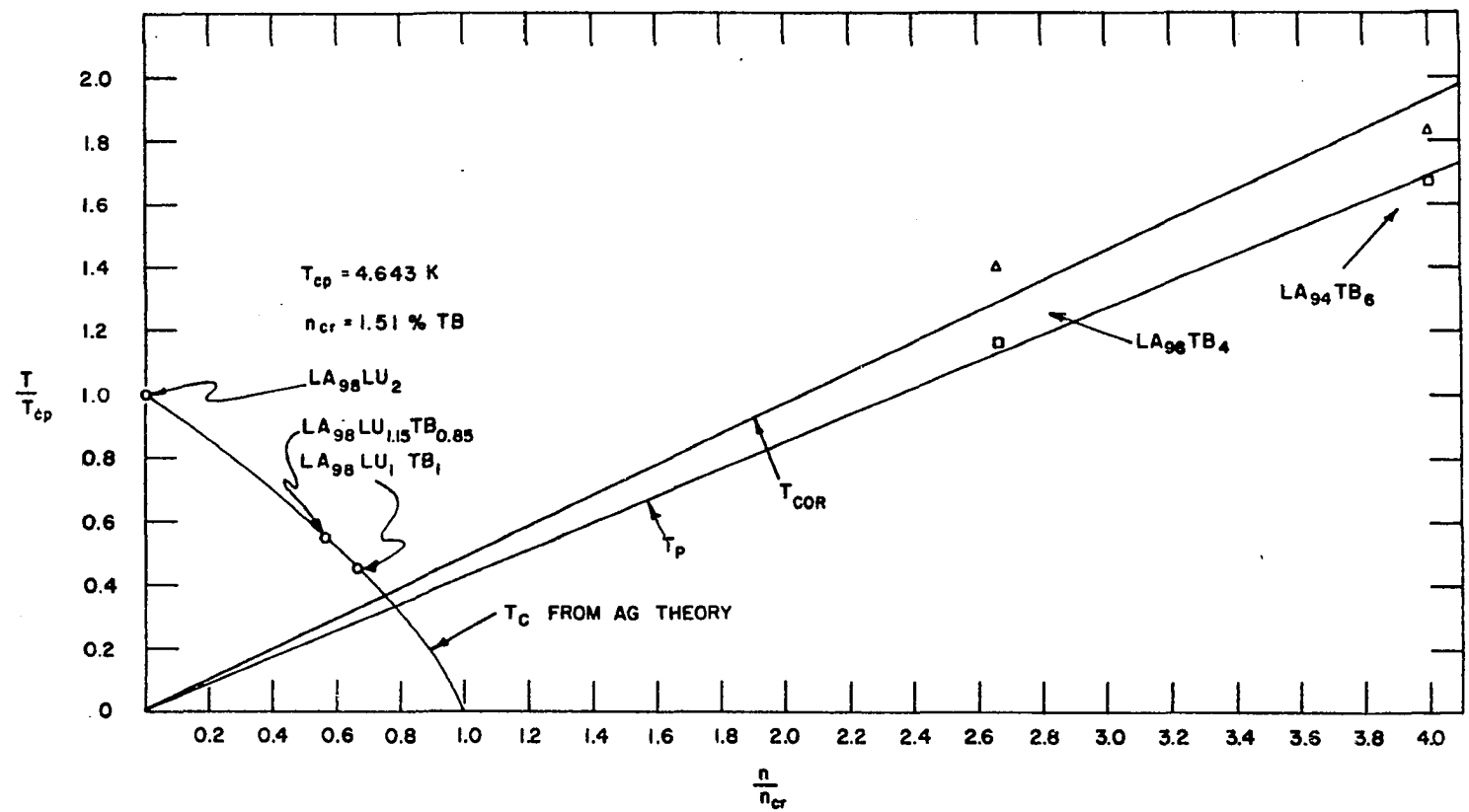

Figure 18. The "coexistence" diagram. T_P is defined as the peak in susceptibility curve and T_{COR} is the temperature at which impurity spin correlations cause the susceptibility to deviate from the Curie-Weiss law. Samples 2 and 3 agree with the AG prediction of T_C within an accuracy of 0.5%.

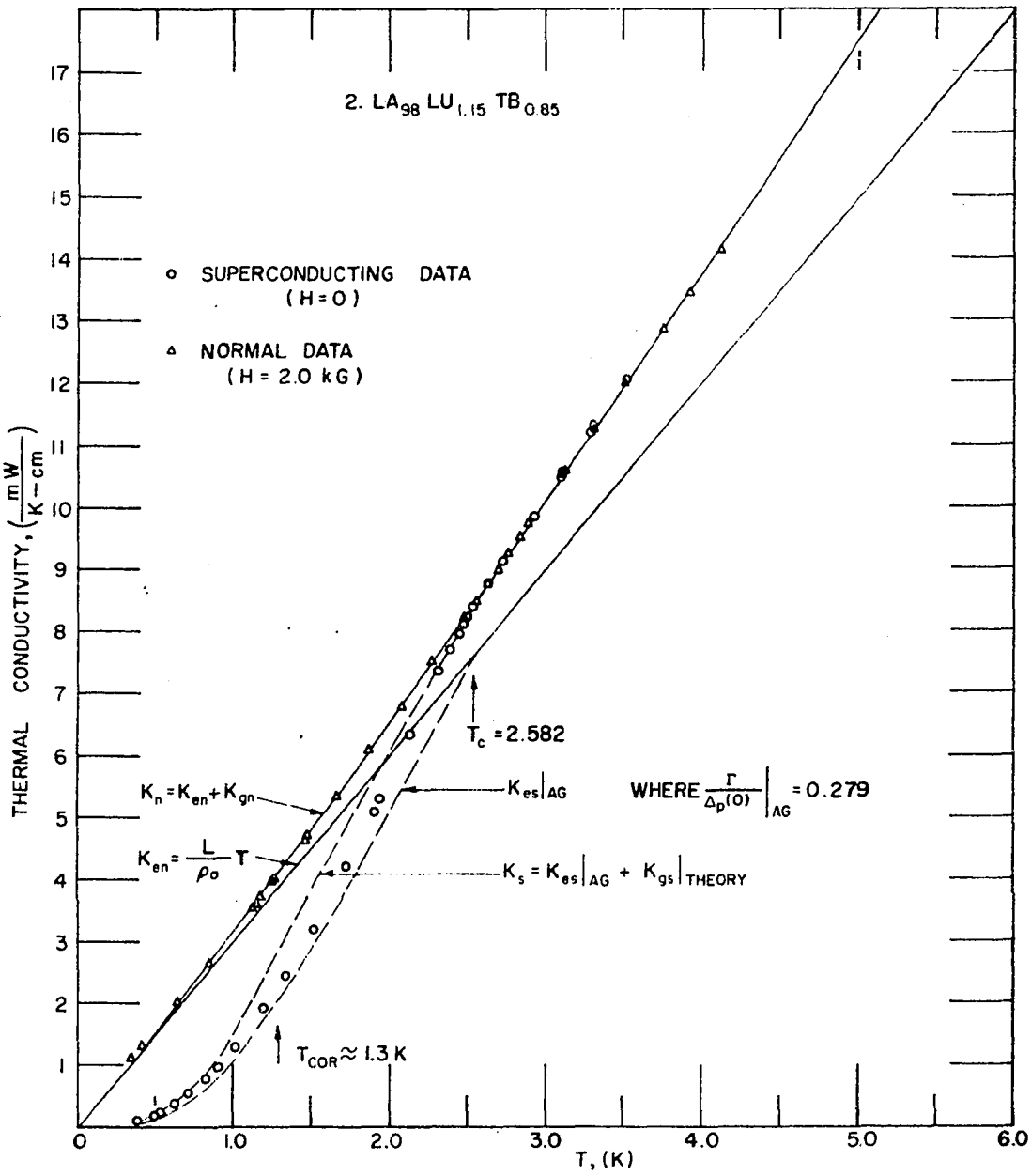

Figure 19. Thermal conductivity data for sample 2. The regions between the solid lines again represents the phonon contribution.

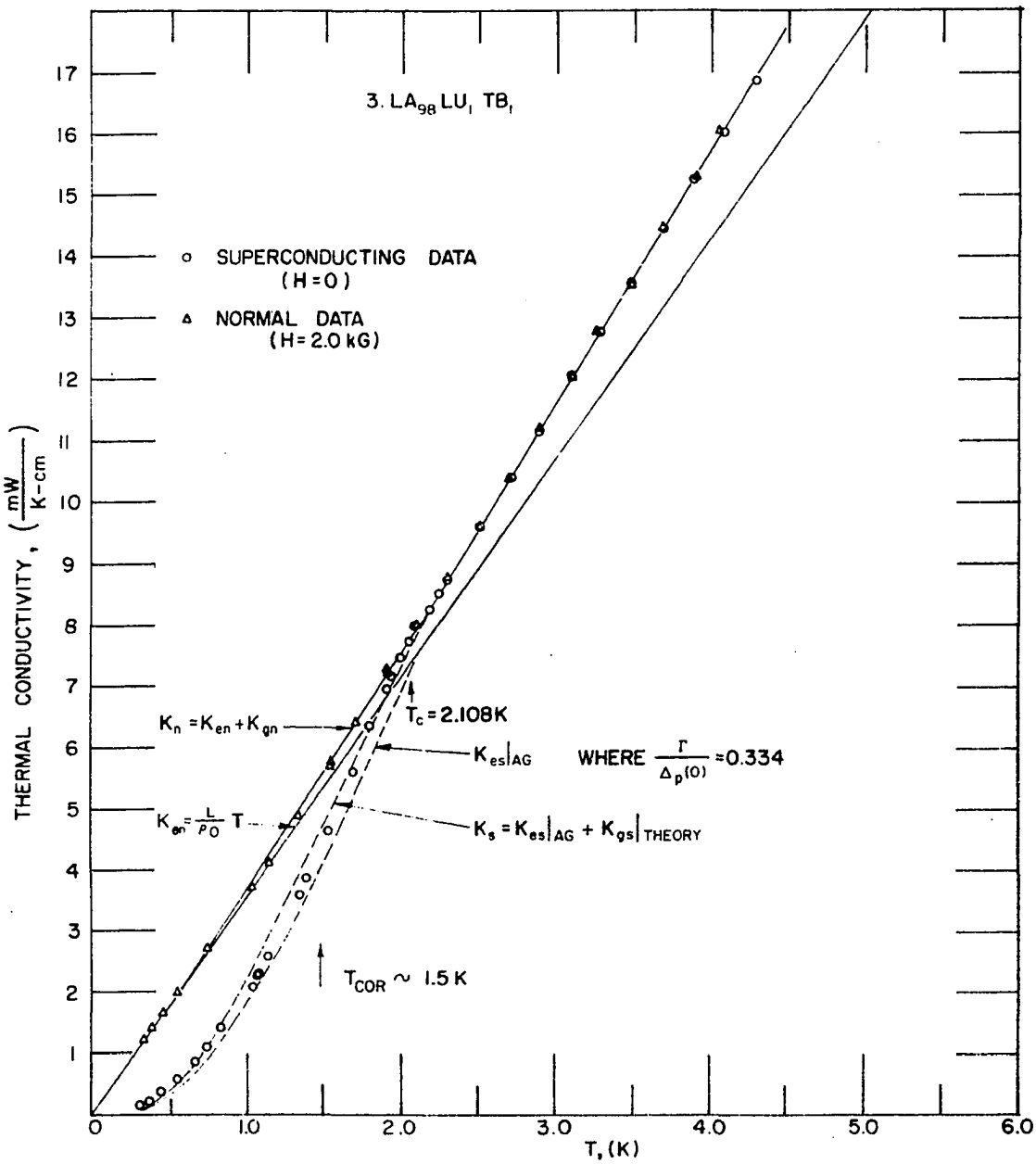

Figure 20. Thermal conductivity data for sample 3.

scattering time (τ_{ex}) of the electrons by the impurity spins when the impurity spins are ordering in the superconducting state. This anomalous temperature dependence (τ_{ex} is temperature independent in AG theory) should be strongly reflected in the electronic thermal conductivity. It is clear from Figures 19 and 20 that there are no dramatic steps in the total conductivity of the type discussed by Bennemann. The ratios K_s/K_n have been plotted (open circles) on Figures 21 and 22 in order to compare them more easily with Bennemanns curve (Figure 1). This plot also shows no kinks or shoulders and in fact the data lie fairly close to the theoretical predictions of Ambegaokar and Griffin (20) for an AG like superconductor with the T_c/T_{cp} ($\Gamma/\Delta_p(0)$) values exhibited by these two samples. A first glance at the raw data does not reveal any effects which might be attributed to magnetic ordering.

The question now arises, however, as to whether there might be phonon contributions which when added to a curve of the form envisaged by Bennemann might give the observed smooth variation of the K_s/K_n data. In the host material the phonons participated in a striking coincidence in that the decrease in K_{es} was compensated for by a corresponding increase in K_{gs} so there was no break from normal state data until T was about 1.5 K below T_c. It is possible that they are involved in another striking coincidence which

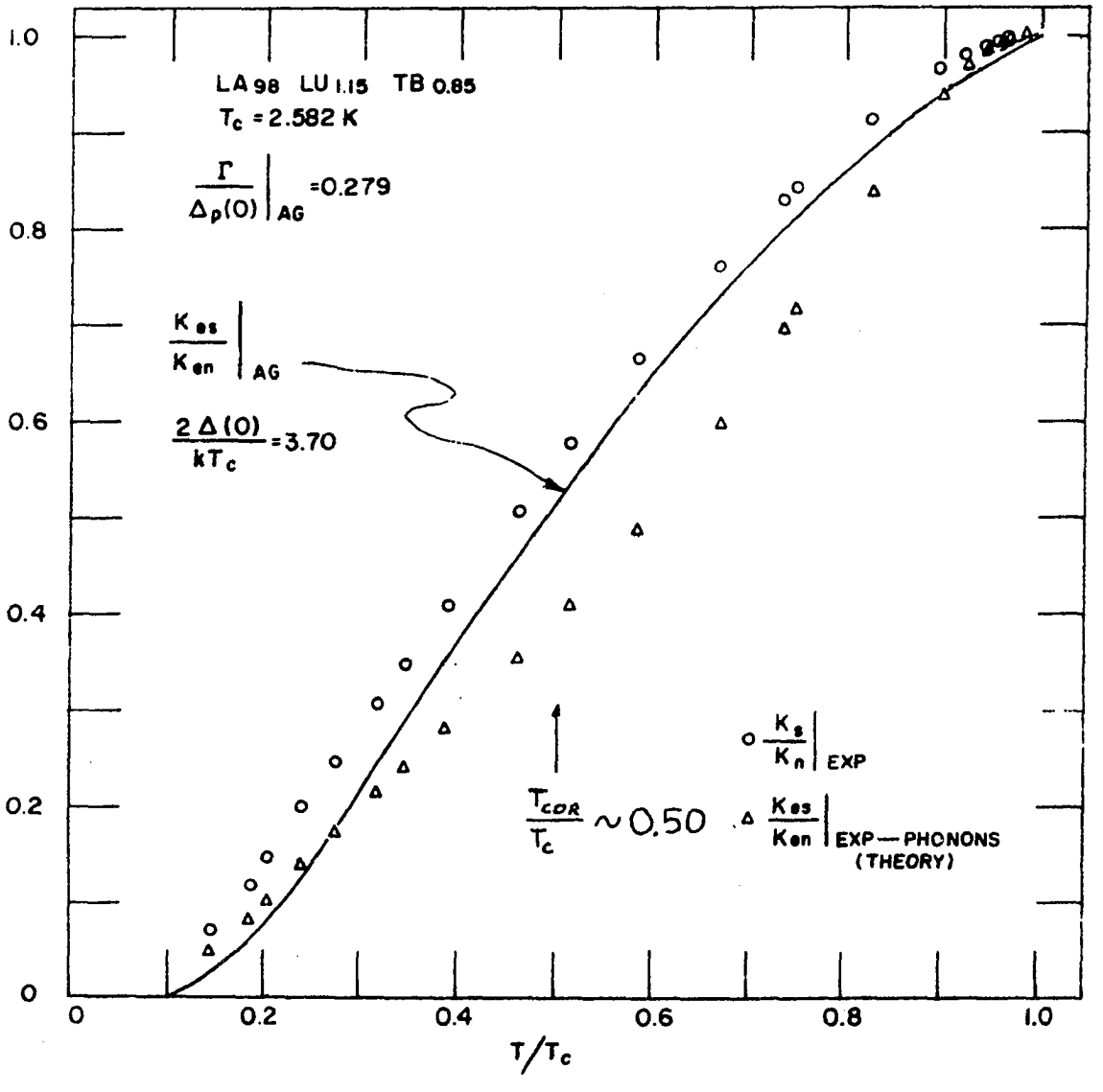

Figure 21. Sample 2. The superconducting and normal state ratios of total thermal conductivity are plotted as circles while the triangles represent the effect of subtracting out the phonon correction term.

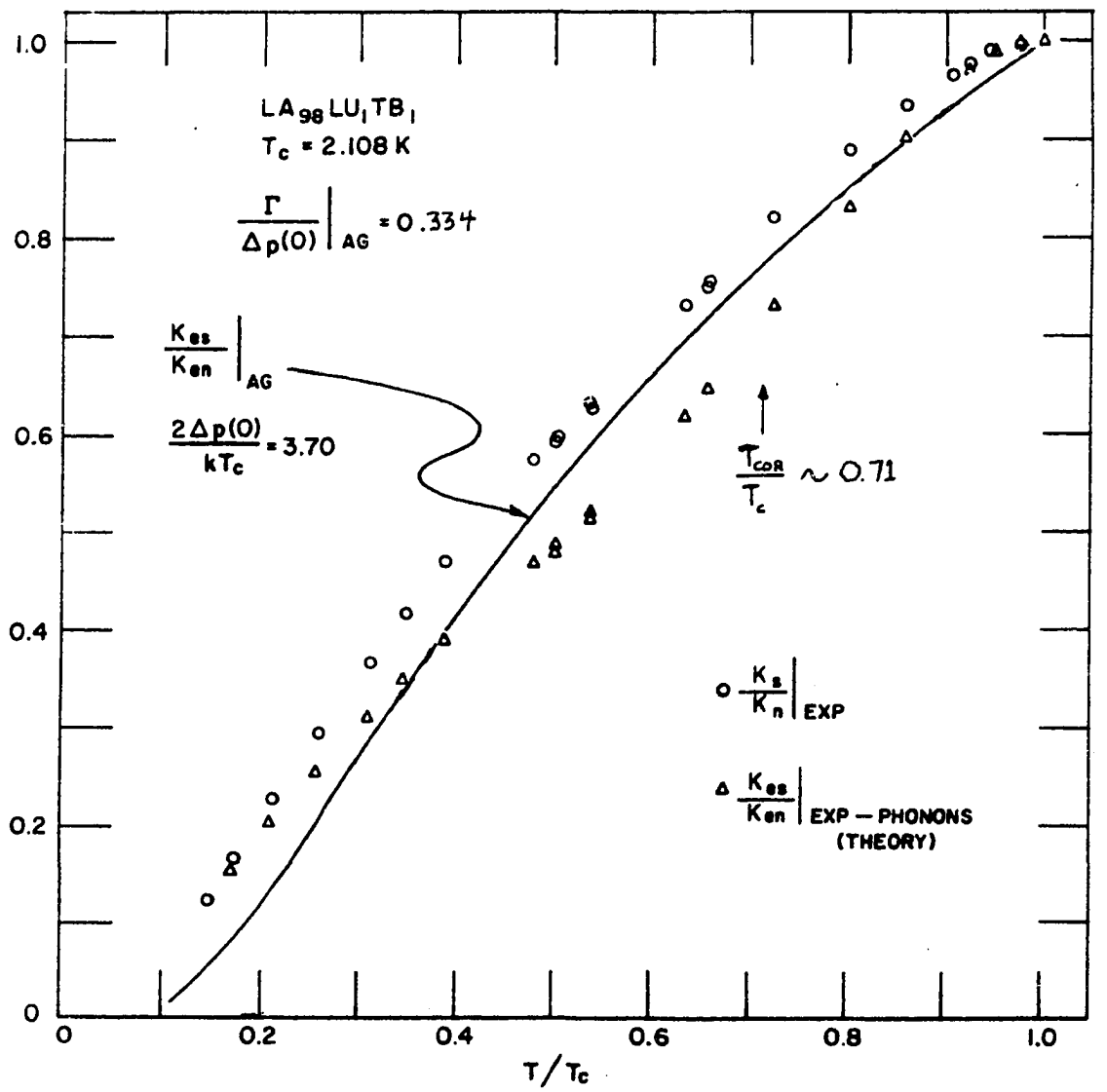

Figure 22. Sample 3. The superconducting and normal state ratios of total thermal conductivity are plotted as circles while the triangles represent the effect of subtracting out the phonon correction term.

might be masking the true magnetic order effect. Unfortunately, as mentioned in the previous chapter, there are so many adjustable parameters in fitting the host thermal conductivity data that one cannot uniquely separate the various components. Even though the analysis of the phonons is not necessarily correct, it at least indicates what might be happening.

Several assumptions have been made in the analysis. We have assumed that the point defect, grain boundary, and dislocation scattering is the same in the alloys as in the host material. In addition we have assumed that R_g for these magnetic impurity doped alloys is the BRT value. The weakness of these assumptions is evident from the previously discussed effects of annealing, but this error is partially compensated for by using the normal state data on samples 2 and 3 to obtain the value of $K_{gn/e} = B_e T^2$. Hence the analysis is forced to agree with the normal state phonon contribution for each sample above T_c. Perhaps a greater error is introduced by using the BRT R_g function for $K_{gs/e}/K_{gn/e}$ but again this is the most reasonable choice possible since no corresponding calculation for an AG R_g function is currently available. Results for this analysis of the phonon conductivity (K_{gs}) for all three samples are shown in Figure 23 and these results are also displayed as the ratios K_{gs}/K_{gn} in Figure 24. The smaller value of the maximum

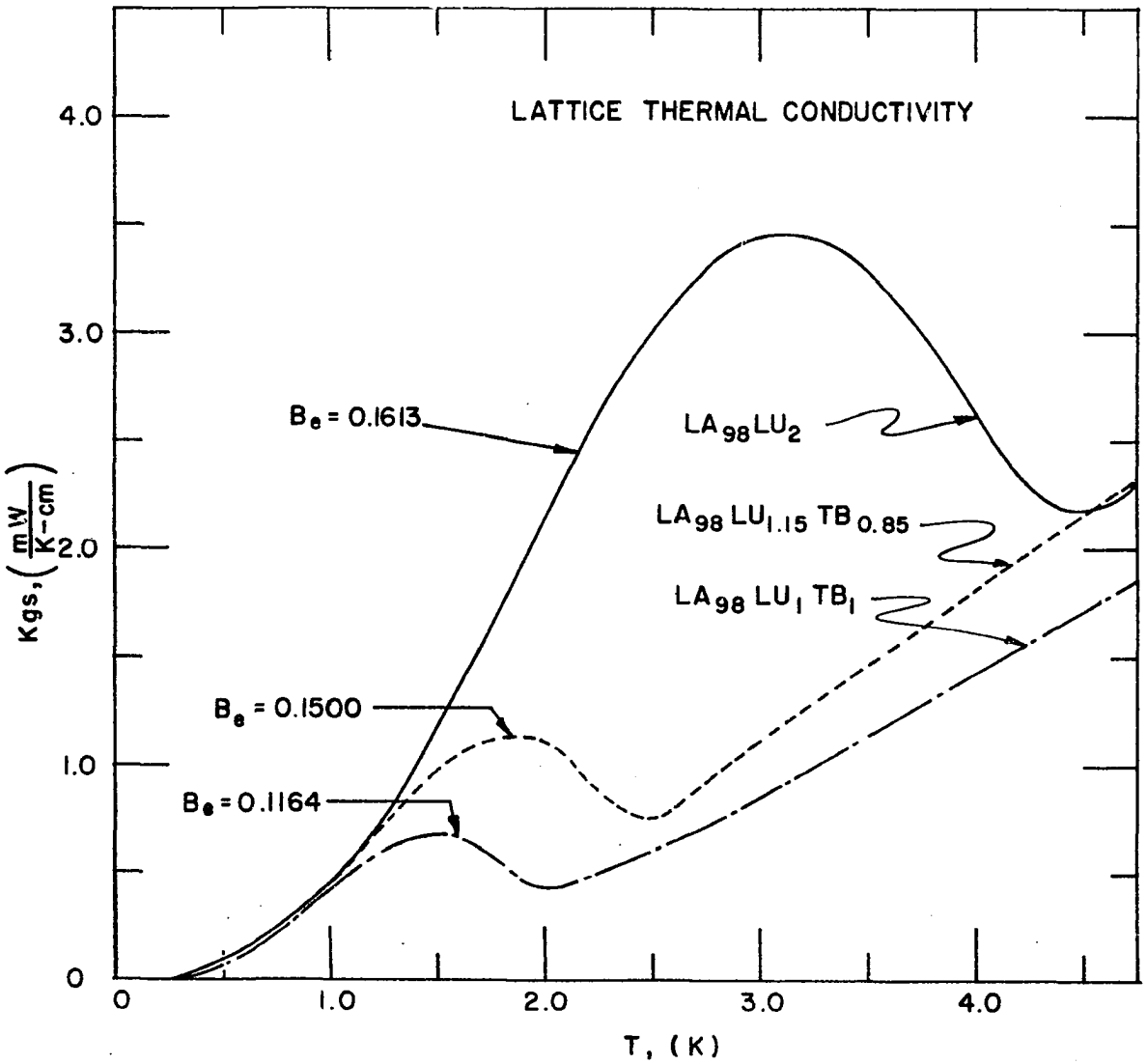

Figure 23. The calculated correction curves for the lattice thermal conductivity.

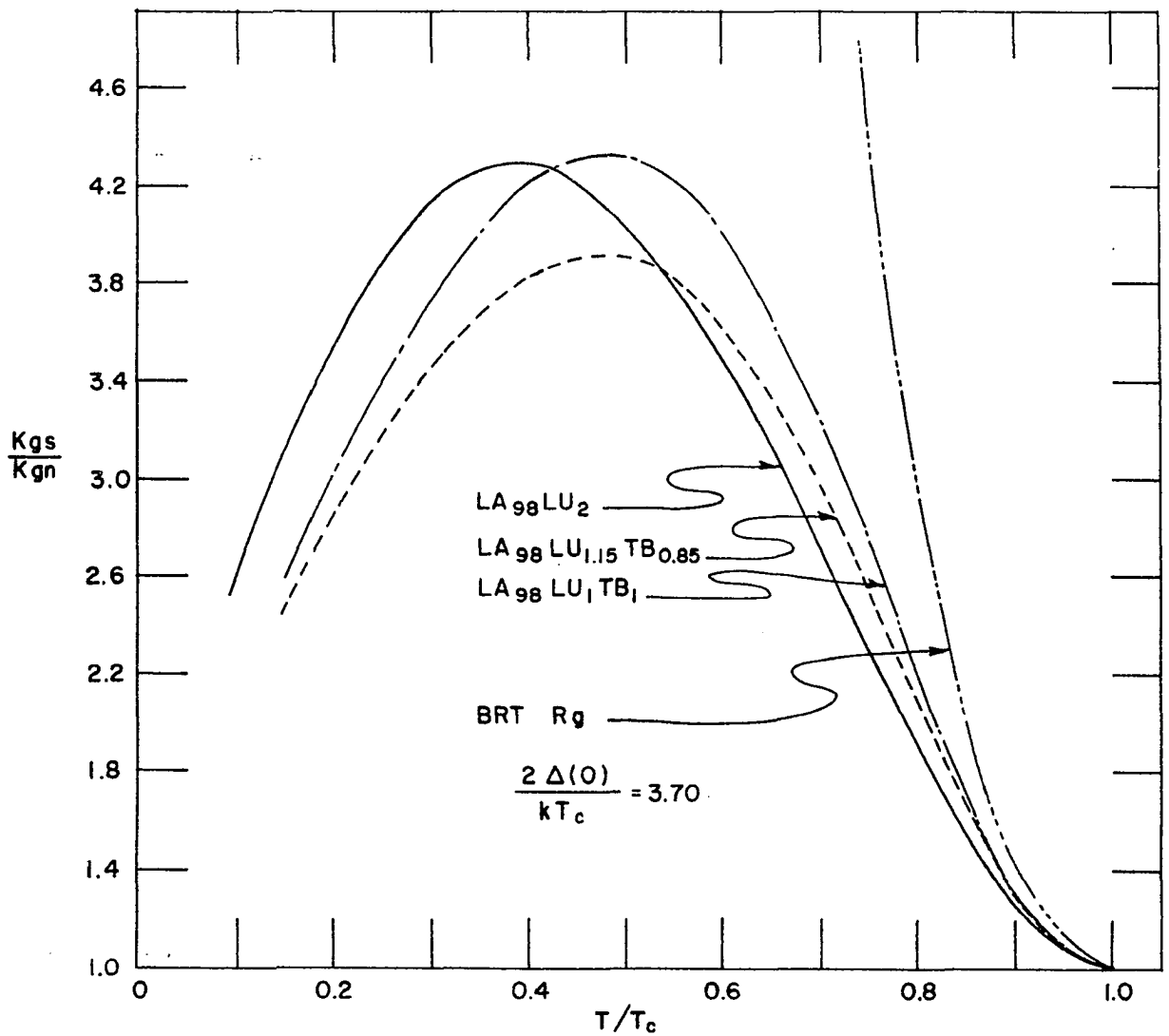

Figure 24. The calculated values of the ratio of superconducting lattice conduction to the normal state value.

ratio for La_{98} $Lu_{1.15}$ $Tb_{0.85}$ is a reflection of the heavier faulting in that sample and hence a smaller fraction of the phonon scattering is caused by electrons. This shows that the analysis partially reflects the effects of annealing.

Results for the electronic conductivity which were obtained by subtracting the calculated phonon terms from the total conductivity are shown in the form

$$\frac{(K_s - K_{gs})}{(K_n - K_{gn})}$$

as triangle on Figure 21 and Figure 22. These data lie substantially below the K_s/K_n curve and are certainly far below the Ambegaokar-Griffin theory. The smaller shoulder at a reduced temperature of about 0.5 is very similar to results observed in the host sample before the "best fit" curve for K_{gs} was obtained. That is, an incorrect phonon analysis can generate shoulders in the $(K_s - K_{gs})/(K_n - K_{gn})$ curve as is evident from the peaks in K_{gs} on Figure 23. On the other hand it is not impossible for the phonon terms to add to a K_{es} anomaly in just the right way so as to obtain the smooth K_s/K_n results.

Another way to cast the results would be to add the phonon conductivity to the Ambegaokar-Griffin theory and compare these results with the directly measured conductivity as shown by the solid line on Figure 19 and Figure 20.

The data lie below the theory at high temperatures and above the theory at low temperatures.

In closing it should be mentioned that the dramatic breaks suggested by Bennemann in Figure 1 were calculated for a concentration equal to 0.9 of the critical concentration. The shoulders might be less dramatic at lower concentrations (sample 2 is 0.56 n_{cr} and sample 3 is 0.66 n_{cr}). The sudden breaks in Figure 1 could also be modified by the proper choice of the spin-orbit relaxation time which would place K_s/K_n somewhere in between the two curves shown by Bennemann. Hence, failure to see the effect in these samples does not necessarily mean that it is not there.

CONCLUDING REMARKS

The purpose of these experiments has been to show whether superconductivity can exist in the presence of magnetic order and to determine the effect of magnetic order on the superconducting properties as reflected in the thermal conductivity.

Susceptibility measurements on normal state properties of the La-Lu-Tb system have indicated that there is some kind of magnetic order at temperature below T = 1.3n where n is the concentration in percent. Single crystal susceptibility measurements have also shown that there is a strong anisotropy in the magnetic ordering and the moments tend to line up in the basal plane of the d-hcp structure. Neutron diffraction powder pattern measurement on samples with 10 and 20 atomic percent Tb show short range order peaks in the forward direction but when the Tb concentration is reduced to 5 atomic percent this short range order peak disappears. For the 5 atomic percent specimen the magnetic scattering below the ordering peak is the same as it was in the paramagnetic state. We conclude from this that the ordering is a local phenomenon associated with the crystal field levels determined by the near neighbor atoms.

Thermal conductivity measurements at low temperatures show K_s/K_n values of less than 0.1 so most of the electrons must be dropping into the superconducting ground state.

This rules out the possibility that the superconductivity is filamentary and shows that it is a real bulk phenomenon. When these alloys are cooled below the superconducting transition temperature the thermal conductivity immediately drops below the normal state conductivity and roughly follows the Ambegaokar-Griffin prediction. As the temperature is further cooled through the "magnetic ordering" temperature there are no dramatic changes in the conductivity. Uncertainties about the phonon contribution preclude an accurate determination of K_{es}/K_{en} and there may be subtle changes in this curve at the ordering temperature. We can, however, say that there are no changes such as a 10% jump in the curve and that the conductivity at low temperature is fairly close to the Ambegaokar-Griffin theory. Failure to see a jump in K_s/K_n is again consistent with the very local crystal field interpretation of the neutron results.

BIBLIOGRAPHY

1. Charles Kittel, Introduction to solid state physics (New York, N.Y., John Wiley and Sons, Inc., 1967), 3rd ed., pp. 227-249.

2. J. Bardeen, L. N. Cooper, and J. R. Schrieffer, Phys. Rev. 108, 1175 (1957).

3. J. R. Schrieffer, Theory of superconductivity (New York, N.Y., W. A. Benjamin, Inc., 1964).

4. P. G. de Gennes, Superconductivity of metals and alloys (New York, N.Y., W. A. Benjamin, Inc., 1966).

5. D. Shoenberg, Superconductivity (Cambridge, England, Cambridge University Press, 1965), 2nd ed.

6. B. T. Matthias, T. H. Geballe, and V. B. Compton, Rev. Mod. Phys. 35, 1 (1963).

7. P. W. Anderson, J. Phys. Chem. Solids 11, 26 (1959).

8. B. T. Matthias, H. Suhl, and E. Corenzwit, Phys. Rev. Letters 1, 92 (1958).

9. B. T. Matthias, H. Suhl, and E. Corenzwit, J. Phys. Chem. Solids 13, 1956 (1959).

10. C. Herring, Physica 24, 5184 (1958).

11. B. T. Matthias and H. Suhl, Phys. Rev. Letters 2, 5 (1959).

12. A. A. Abrikosov and L. P. Gor'kov, Zh. Eksperim. i Teor. Fiz. 39, 1781 (1960) [English transl.: Soviet Phys.--JETP 12, 1243 (1961)].

13. Kazumi Maki and Peter Fulde, Phys. Rev. 140, A1586 (1965).

14. M. B. Maple (to be published).

15. F. Reif and M. A. Woolf, Phys. Rev. Letters 9, 315 (1962).

16. J. Millstein and M. Tinkham, Phys. Rev. 158, 325 (1967).

17. Wayne R. Decker. Critical field curves for superconductors with magnetic impurities. Unpublished Ph.D. thesis. Ames, Iowa, Library, Iowa State University. 1968.

18. S. Skalski, O. Betbeder-Matibet, and P. R. Weiss, Phys. Rev. 136, A1500 (1964).

19. L. P. Kadanoff and I. I. Falko, Phys. Rev. 136, A1170 (1964).

20. V. Ambegaokar and A. Griffin, Phys. Rev. 137, A1151 (1965).

21. K. Maki and P. Fulde, Phys. Rev. 140, A1586 (1965).

22. J. M. Mochel and R. D. Parks, Phys. Rev. Letters 16, 1156 (1966).

23. R. L. Cappelletti and D. K. Finnemore (to be published in Phys. Rev.).

24. B. T. Matthias, H. Suhl, and E. Corenzwit, Phys. Rev. Letters 1, 449 (1958).

25. R. A. Hein, R. L. Falge, Jr., B. T. Matthias, and C. Corenzwit, Phys. Rev. Letters 2, 500 (1959).

26. H. Suhl, B. T. Matthias, and E. Corenzwit, J. Phys. Chem. Solids 11, 346 (1959).

27. J. E. Crow and R. D. Parks, Phys. Rev. Letters 21, 378 (1966).

28. R. P. Guertin and R. D. Parks, Solid State Communications 7, 59 (1969).

29. D. K. Finnemore, D. C. Hopkins, and P. E. Palmer, Phys. Rev. Letters 15, 89 (1965).

30. N. E. Phillips and B. T. Matthias, Phys. Rev. 121, 105 (1961).

31. L. P. Gor'kov and A. I. Rusinov. Zh Eksperim. i Teor Fiz. 46, 1363 (1964)[English transl.: Soviet Phys.-- JETP 19, 922 (1964)].

32. K. H. Bennemann and S. Nakajima, Phys. Rev. Letters 16, 243 (1966).

33. K. H. Bennemann, Phys. Rev. Letters 17, 438 (1966).

34. P. W. Anderson and H. Suhl, Phys. Rev. 116, 898 (1959).

35. M. A. Ruderman and C. Kittel, Phys. Rev. 96, 99 (1954).

36. T. Kasuya, Progr. Theoret. Phys. (Kyoto) 16, 45 (1956).

37. K. Yosida, Phys. Rev. 106, 893 (1957).

38. S. H. Liu, J. Phys. Chem. Solids 24, 475 (1963).

39. J. Owen, M. E. Browne, V. Arp, and A. F. Kip, J. Phys. Chem. Solids 2, 85 (1957).

40. M. W. Klein, Phys. Rev. Letters 16, 90 (1966).

41. M. W. Klein, Phys. Rev. 141, 489 (1966).

42. M. W. Klein and R. Brout, Phys. Rev. 132, 2412 (1963).

43. M. Marshall, Phys. Rev. 118, 1520 (1960).

44. S. H. Liu, Phys. Rev. 157, 411 (1967).

45. D. K. Finnemore, L. J. Williams, F. H. Spedding, and D. C. Hopkins, Phys. Rev. 176, 712 (1968).

46. K. H. Bennemann, J. W. Garland, and F. M. Mueller, Phys. Rev. Letters 23, 169 (1969).

47. K. H. Bennemann and F. M. Mueller, Phys. Rev. 176, 546 (1968).

48. B. T. Matthias and H. Suhl, Phys. Rev. 114, 977 (1959).

49. E. N. Hopkins, D. T. Peterson, and H. H. Baker (to be published).

50. G. E. Bacon, Neutron diffraction (London, England, Oxford University Press, 1955).

51. K. W. Taconis, Progress in low temperature physics Vol. III (Amsterdam, North Holland Publishing Company, 1961).

52. W. C. Black, Jr., W. R. Roach, and J. C. Wheatley, Rev. Sci. Instr. 35, 587 (1964).

53. J. S. Rogers, R. J. Tanish, M. S. Anderson, and C. A. Swenson, Metrologia 4, 47 (1968).

54. A. C. Anderson, W. Reese, and J. C. Wheatley, Rev. Sci. Instr. 34, 1386 (1963).

55. C. A. Schiffman, J. F. Cochran, and M. Garber, J. Phys. Chem. Solids 24, 1369 (1963).

56. R. Berman, Proc. Roy. Soc. 208, A90 (1951).

57. R. Berman, In Experimental cryophysics, edited by F. E. Hoare, L. C. Jackson, and N. Kurti (London, England, Butterworth and Co., Ltd., 1961), pp. 327-336.

58. J. Bardeen, G. Rickayzen, and L. Tewordt, Phys. Rev. 113, 982 (1959).

59. P. Lindenfeld and W. B. Pennebaker, Phys. Rev. 127, 1881 (1962).

60. C. B. Satterthwaite, Phys. Rev. 125, 873 (1962).

61. P. Lindenfeld and H. Rohrer, Phys. Rev. 139, A206 (1965).

62. J. B. Sousa, J. Phys. C (Solid State Phys.) 2, 629 (1969).

63. P. G. Klemens, Proc. Roy. Soc. (London) A208, 108 (1951).

64. P. G. Klemens, Proc. Roy. Soc. (London) A68, 1113 (1955).

65. Glen A. Slack, Phys. Rev. 105, 832 (1957).

66. P. G. Klemens and L. Tewordt, Rev. Mod. Phys. 36, 118 (1964).

67. Ronald J. Sladek, Phys. Rev. 97, 902 (1955).

68. G. T. Fox, M. W. Wolfmeyer, and J. R. Dillinger, Phys. Rev. 177, 177 (1969).

69. A. B. Pippard, Phil. Mag. 46, 1104 (1955).

70. D. L. Johnson and D. K. Finnemore, Phys. Rev. 158, 376 (1967).

ACKNOWLEDGMENTS

The author would like to thank Professor D. K. Finnemore and the members of his group (in particular Mr. J. Ostenson) for their help in completing this project.

Thanks are also due to Dr. W. R. Decker for his aid in taking some of the data.

Finally he would like to express special gratitude to Professor Finnemore for his aid in excluding the author from the rather large (32% in 1968) group of Ph.D.'s who went on relief after completing their degree requirements.

APPENDIX A

Table 7. The fit constants for GR-928

	Below 1 K	Above 1 K
Q(1)	$0.66992799640721 \times 10^{2}$	$0.45012462320976 \times 10^{3}$
Q(2)	$-0.44314887389498 \times 10^{2}$	$-0.57716701640176 \times 10^{3}$
Q(3)	$0.12221312647641 \times 10^{2}$	$0.30766216728464 \times 10^{3}$
Q(4)	$-0.17899874477756 \times 10^{1}$	$-0.86626108845608 \times 10^{2}$
Q(5)	$0.14524040340511 \times 10^{0}$	$0.13567336692413 \times 10^{2}$
Q(6)	$-0.61330252213404 \times 10^{-2}$	$-0.11215901813746 \times 10^{1}$
Q(7)	$0.10383791467001 \times 10^{-3}$	$0.38287320571341 \times 10^{-1}$

Table 8. Calibration data for GR-928

T, (K)	R, (ohms)
4.1733	60.17
4.0991	61.05
4.0574	61.73
4.0233	62.12
3.9956	62.54
3.9389	63.25
3.8482	64.64
3.7843	65.58
3.7567	65.99
3.7267	66.45

Table 8 (Continued)

T, (K)	R, (ohms)
3.6695	67.31
3.5984	68.54
3.5261	69.72
3.4424	71.21
3.3336	73.16
3.2358	75.09
3.2751	74.33
3.1607	76.68
3.0964	78.00
3.0407	79.26
2.9961	80.23
2.9202	81.99
2.8482	83.78
2.7045	87.60
2.5651	91.76
2.5031	93.67
2.4334	95.92
2.3564	98.74
2.2557	102.64
2.2381	102.53
2.1500	107.24
2.0980	109.68

Table 8 (Continued)

T, (K)	R, (ohms)
2.0803	110.49
2.0754	110.77
1.9974	114.77
1.9833	115.54
1.9567	117.04
1.9283	118.65
1.8128	125.88
1.8112	126.12
1.6175	141.33
1.6107	142.02
1.7079	133.70
1.6375	139.56
1.6293	140.37
1.5039	152.94
1.4000	166.06
1.3950	166.75
1.3773	169.09

Table 9. Susceptibility data

Sample 1		Sample 2		Sample 3	
T (K)	M (Arbitrary)	T (K)	M (Arbitrary)	T (K)	M (Arbitrary)
~6	5717	~6	4038	~5.7	4201
~5.7	5677	~5.7	4058	~4.9	4206
~5.4	5350	~5.4	4064	4.0	4214
4.98	4600	5.007	4075	2.88	4229
4.95	4550	4.026	4112	2.317	4232
4.875	4440	3.480	4132	2.218	4181
4.755	4265	3.021	4145	2.171	4085
4.722	4181	2.863	4116	2.126	3457
4.682	4014	2.815	4081	2.116	3005
4.664	3520	2.734	2961	2.105	2502
4.655	3294	2.695	3842	2.095	2067
4.654	2630	2.674	3716	2.085	1701
4.640	-0550	2.645	3415	2.075	1471
4.626	-3840	2.628	2892	2.059	1271
4.617	-4334	2.615	2446	2.045	1193
4.606	-4665	2.600	0976	2.030	1152
4.595	-4781	2.591	-0262	2.015	1131
4.575	-4845	2.578	-1835	2.002	1116
4.556	-4903	2.563	-4120	1.985	1105
4.545	-4948	2.551	-5227	1.965	1093
4.490	-4993	2.536	-5925	1.940	1082

Table 9 (Continued)

Sample 1		Sample 2		Sample 3	
T (K)	M (Arbitrary)	T (K)	M (Arbitrary)	T (K)	M (Arbitrary)
4.451	-5007	2.521	-6431	1.913	1076
4.312	-5022	2.498	-6882	1.884	1073
4.15	-5022	2.476	-7126	1.853	1071
3.95	-5023	2.448	-7257	1.793	1065
3.81	-5023	2.422	-7312	1.694	1065
3.54	-5023	2.396	-7341	1.599	1064
3.48	-5023	2.359	-7365	0.35	1067
3.14	-5023	2.009	-7402		
2.09	-5023	1.732	-7402		
1.49	-5023	1.34	-7402		
1.40	-5029	1.06	-7404		
0.77	-5027				
0.61	-5025				

APPENDIX B

The tables which follow present the experimentally determined values of K_s, K_n, and T for samples 1, 2, and 3. Temperature is measured in Kelvins and thermal conductivity is measured in mW/(K - cm).

Since K_s and K_n were measured at different temperatures the ratio K_s/K_n was obtained by dividing the experimental value of K_s by an interpolated value of K_n. The interpolation was obtained by a least square fit of

$$K_n = \sum_{N=1}^{6} Q(N)T^{N-1}$$

to the experimental K_n data.

Table 10. Sample 1 La_{98} Lu_2 H = 0

T	K_s	K_s-K_{gs}|Theory	K_{gs}|Theory
4.085	11.2095	8.7063	2.5031
3.882	10.6186	7.8180	2.8005
3.814	10.3838	7.4828	2.9010
3.794	10.3613	7.4324	2.9289
3.705	10.1082	7.0562	3.0520
3.624	9.8615	6.7079	3.1535
3.535	9.5600	6.3098	3.2502
3.498	9.3798	6.0946	3.2852
3.440	9.2763	5.9420	3.3343
3.352	8.9888	5.5960	3.3927
3.351	8.9357	5.5423	3.3934
3.165	8.2947	4.8403	3.4544
3.015	7.7529	4.3107	3.4421
2.794	6.8903	3.5624	3.3278
2.470	5.4926	2.5292	2.9635
2.297	4.6936	2.0077	2.6859
2.160	4.0920	1.6554	2.4367
2.017	3.4257	1.2642	2.1615
1.732	2.2520	0.6481	1.6039
1.701	2.1248	0.5820	1.5429
1.409	1.1960	0.1924	1.0035
1.182	0.6904	0.0377	0.6527
1.042	0.4729	-0.0021	0.4750
0.970	0.3909	-0.0046	0.3955
0.845	0.2649	-0.0113	0.2761
0.703	0.1627	-0.0070	0.1696
0.589	0.1045	-0.0011	0.1056
0.473	0.0598	0.0020	0.0578
0.447	0.0529	0.0036	0.0493

Table 11. Sample 1 La_{98} Lu_2 H = 11k0e

T	K_n	$K_n - K_{gn}$|Theory	K_{gn}|Theory
4.273	11.8777	9.8943	1.9833
3.988	10.9962	9.2091	1.7871
3.705	10.1327	8.5442	1.5886
3.285	8.8651	7.5708	1.2943
3.067	8.2289	7.0847	1.1442
2.849	7.5953	6.5964	0.9990
2.491	6.5442	5.7705	0.7737
2.288	5.9351	5.2799	0.6552
2.068	5.2873	4.7515	0.5358
2.029	5.1975	4.6821	0.5155
1.842	4.6528	4.2293	0.4235
1.666	4.1597	3.8151	0.3447
1.484	3.6515	3.3805	0.2710
1.376	3.3684	3.1369	0.2315
1.323	3.2204	3.0073	0.2130
1.320	3.2210	3.0091	0.2118
1.224	2.9725	2.7918	0.1807
1.215	2.9489	2.7711	0.1778
1.051	2.5335	2.4030	0.1305
0.979	2.3469	2.2350	0.1119
0.896	2.1505	2.0580	0.0925
0.897	2.1474	2.0549	0.0925
0.820	1.9599	1.8838	0.0761
0.815	1.9505	1.8754	0.0751
0.732	1.7475	1.6882	0.0593
0.633	1.5199	1.4770	0.0429
0.629	1.4994	1.4570	0.0424
0.578	1.3726	1.3376	0.0350
0.490	1.1673	1.1431	0.0241
0.477	1.1352	1.1125	0.0227
0.477	1.1371	1.1145	0.0227
0.374	0.8986	0.8858	0.0129
0.347	0.8219	0.8111	0.0108
0.353	0.8362	0.8250	0.0112

Table 12. Sample 1 La_{98} Lu_2

$\frac{T}{T_c}$	$\frac{K_s}{K_n}$	$\frac{K_s-K_{gs}\mid Theory}{K_n-K_{gn}\mid Theory}$	$\frac{K_{gs}}{K_{gn}\mid Theory}$
0.8797	0.99342	0.92635	1.34989
0.8361	0.99609	0.87527	1.63472
0.8214	0.99327	0.85271	1.74203
0.8172	0.99666	0.85129	1.77322
0.7980	0.99799	0.82766	1.92079
0.7805	0.99746	0.80443	2.05880
0.7614	0.99350	0.77572	2.21237
0.7535	0.98594	0.75714	2.27624
0.7409	0.99310	0.75070	2.37778
0.7220	0.98978	0.72547	2.52996
0.7218	0.98432	0.71877	2.53204
0.6816	0.97281	0.66472	2.85232
0.6493	0.95916	0.62143	3.10322
0.6018	0.92746	0.55410	3.45423
0.5321	0.84878	0.44493	3.89244
0.4948	0.78727	0.37982	4.06739
0.4652	0.73592	0.33310	4.17085
0.4344	0.66554	0.27242	4.24494
0.3731	0.51873	0.16259	4.29385
0.3664	0.49938	0.14867	4.28715
0.3035	0.34561	0.05934	4.12472
0.2545	0.24106	0.01388	3.89412
0.2244	0.18854	-0.00088	3.71090
0.2089	0.16790	-0.00205	3.60432
0.1819	0.13114	-0.00579	3.39735
0.1514	0.09707	-0.00432	3.12777
0.1270	0.07441	-0.00081	2.88275
0.1019	0.05302	0.00184	2.59994
0.0962	0.04966	0.00346	2.53152

Table 13. Sample 2 La_{98} $Lu_{1.15}$ $Tb_{0.85}$ H = 0

T	K_s	K_s-K_{gs}|Theory	K_{gs}|Theory
2.544	8.3848	7.6190	0.7658
2.501	8.2098	7.4572	0.7525
2.474	8.0963	7.3446	0.7517
2.442	7.9364	7.1792	0.7572
2.391	7.6909	6.9131	0.7778
2.325	7.3409	6.5192	0.8216
2.321	7.3233	6.4985	0.8248
2.139	6.3400	5.3459	0.9941
1.943	5.2834	4.1524	1.1310
1.908	5.0985	3.9563	1.1422
1.735	4.2179	3.0870	1.1309
1.518	3.1979	2.2098	0.9881
1.336	2.4286	1.6307	0.7978
1.197	1.8968	1.2610	0.6358
1.011	1.2821	0.8505	0.4316
0.902	0.9728	0.6480	0.3248
0.827	0.7867	0.5272	0.2595
0.716	0.5453	0.3676	0.1777
0.629	0.3873	0.2619	0.1255
0.532	0.2414	0.1618	0.0796
0.485	0.1796	0.1179	0.0617
0.378	0.0833	0.0523	0.0310

Table 14. Sample 2 La_{98} $Lu_{1.15}$ $Tb_{0.85}$ H = 0

T	K_n	$K_{n-}K_{gn}$|Theory	K_{gn}|Theory
3.520	12.0439	10.6613	1.3826
3.305	11.2290	9.9906	1.2384
3.300	11.1760	9.9407	1.2352
3.127	10.5659	9.4441	1.1218
3.127	10.5567	9.4353	1.1215
3.109	10.5052	9.3954	1.1098
3.102	10.4635	9.3578	1.1057
2.929	9.8279	8.8333	0.9945
2.731	9.1096	8.2374	0.8722
2.634	8.7398	7.9255	0.8143

Table 15. Sample 2 La_{98} $Lu_{1.15}$ $Tb_{0.85}$ H = 2k0e

T	K_n	K_n-K_{gn}|Theory	K_{gn}|Theory
4.130	14.1161	12.3231	1.7930
3.927	13.4109	11.7540	1.6569
3.751	12.8293	11.2913	1.5380
3.521	11.9603	10.5770	1.3833
3.511	11.9556	10.5790	1.3766
3.305	11.1931	9.9547	1.2384
3.300	11.2106	9.9753	1.2353
3.127	10.5570	9.4355	1.1215
3.112	10.4813	9.3696	1.1117
3.109	10.5108	9.4006	1.1102
2.907	9.7419	8.7609	0.9810
2.840	9.4833	8.5441	0.9392
2.766	9.2176	8.3242	0.8934
2.697	8.9711	8.1192	0.8518
2.633	8.7422	7.9288	0.8134
2.550	8.4485	7.6833	0.7651
2.489	8.2197	7.4901	0.7296
2.285	7.4969	6.8798	0.6171
2.080	6.7734	6.2616	0.5118
1.883	6.0758	5.6571	0.4187
1.672	5.3473	5.0193	0.3280
1.482	4.6993	4.4438	0.2555
1.457	4.6191	4.3724	0.2467
1.275	4.0086	3.8222	0.1864
1.257	3.9454	3.7646	0.1808
1.182	3.6989	3.5402	0.1587
1.133	3.5425	3.3973	0.1452
0.850	2.6460	2.5678	0.0783
0.640	2.0011	1.9592	0.0419
0.419	1.3027	1.2866	0.0161
0.341	1.1047	1.0947	0.0099

Table 16. Sample 2 La_{98} $Lu_{1.15}$ $Tb_{0.85}$

$\frac{T}{T_c}$	$\frac{K_s}{K_n}$	$\frac{K_s-K_{gs}\mid Theory}{K_n-K_{gn}\mid Theory}$	$\frac{K_{gs}}{K_{gn}\mid Theory}$
0.9851	0.99578	1.00112	1.00603
0.9685	0.99330	0.99668	1.02175
0.9583	0.99096	0.99207	1.04183
0.9456	0.98563	0.98274	1.07707
0.9260	0.97726	0.96638	1.15267
0.9004	0.96168	0.93718	1.28644
0.8989	0.96119	0.93581	1.29583
0.8283	0.90958	0.83548	1.83716
0.7524	0.84102	0.71434	2.53591
0.7388	0.82774	0.69315	2.65763
0.6719	0.75837	0.59472	3.19418
0.5881	0.66285	0.48640	3.67558
0.5176	0.57620	0.40782	3.87640
0.4636	0.50517	0.35210	3.89799
0.3916	0.40676	0.28111	3.79171
0.3493	0.34701	0.24009	3.65118
0.3201	0.30663	0.21317	3.52483
0.2772	0.24560	0.17164	3.30811
0.2435	0.19839	0.13922	3.11463
0.2059	0.14552	0.10169	2.87600
0.1877	0.11832	0.08129	2.75106
0.1465	0.06918	0.04618	2.44439

Table 17. Sample 3 La_{98} Lu_1 Tb_1 H = 0

T	K_s	K_s-K_{gs} | Theory	K_{gs} | Theory
2.057	7.7506	7.3375	0.4131
2.000	7.4749	7.0621	0.4128
1.947	7.1788	6.7505	0.4283
1.914	6.9687	6.5249	0.4438
1.811	6.3504	5.8400	0.5103
1.692	5.6112	5.0150	0.5962
1.528	4.6475	3.9819	0.6657
1.389	3.8700	3.2142	0.6558
1.388	3.8539	3.1982	0.6557
1.340	3.6069	2.9683	0.6386
1.339	3.5965	2.9582	0.6383
1.136	2.5969	2.0871	0.5097
1.136	2.6201	2.1104	0.5097
1.065	2.3157	1.8642	0.4515
1.065	2.2885	1.8376	0.4510
1.015	2.1063	1.6974	0.4089
0.825	1.3926	1.1393	0.2534
0.737	1.1035	0.9131	0.1905
0.657	0.8637	0.7229	0.1408
0.547	0.5806	0.4947	0.0860
0.451	0.3737	0.3232	0.0504
0.367	0.2293	0.2009	0.0284
0.316	0.1568	0.1381	0.0187

Table 18. Sample 3 La_{98} Lu_1 Tb_1 H = 0

T	K_n	K_n-K_{gn} | Theory	K_{gn} | Theory
4.428	17.4129	15.7487	1.6642
4.079	16.0384	14.5763	1.4621
3.889	15.2700	13.9184	1.3516
3.690	14.4564	13.2203	1.2360
3.482	13.5862	12.4698	1.1165
3.280	12.7807	11.7774	1.0033
3.099	12.0455	11.1417	0.9038
2.894	11.1741	10.3786	0.7955
2.702	10.3865	9.6885	0.6980
2.511	9.5975	8.9921	0.6054
2.242	8.5240	8.0395	0.4845
2.304	8.7580	8.2468	0.5112
2.176	8.2610	7.8047	0.4563
2.113	7.9803	7.5499	0.4304
2.113	7.9982	7.5678	0.4304

Table 19. Sample 3 La_{98} Lu_1 Tb_1 H = 2.0kOe

T	K_n	K_n-K_{gn}|Theory	K_{gn}|Theory
4.074	16.0441	14.5852	1.4589
3.886	15.2873	13.9374	1.3498
3.688	14.4748	13.2401	1.2347
3.484	13.5681	12.4500	1.1181
3.282	12.7806	11.7766	1.0040
3.100	12.0390	11.1344	0.9046
2.895	11.1896	10.3939	0.7957
2.690	10.3440	9.6520	0.6919
2.510	9.6049	8.9999	0.6051
2.305	8.7703	8.2586	0.5117
2.113	8.0000	7.5695	0.4305
2.111	8.1363	7.7067	0.4296
1.922	7.2875	6.9319	0.3556
1.922	7.2382	6.8826	0.3556
1.715	6.4064	6.1244	0.2820
1.714	6.4177	6.1359	0.2818
1.540	5.6967	5.4705	0.2262
1.540	5.7315	5.5054	0.2261
1.328	4.8808	4.7145	0.1663
1.327	4.8670	4.7009	0.1661
1.137	4.1178	3.9976	0.1202
1.137	4.1531	4.0329	0.1202
1.031	3.7624	3.6647	0.0976
1.030	3.7192	3.6218	0.0974
0.744	2.7150	2.6664	0.0486
0.544	1.9861	1.9616	0.0245
0.449	1.6452	1.6292	0.0160
0.378	1.4047	1.3939	0.0108
0.314	1.2157	1.2086	0.0071

Table 20. Sample 3 La_{98} Lu_2

$\frac{T}{T_c}$	$\frac{K_s}{K_n}$	$\frac{K_s-K_{gs}\mid \text{Theory}}{K_n-K_{gn}\mid \text{Theory}}$	$\frac{K_{gs}}{K_{gn}\mid \text{Theory}}$
0.9760	0.99380	0.99705	1.01264
0.9489	0.98766	0.98707	1.07081
0.9236	0.97621	0.96931	1.17329
0.9080	0.96503	0.95303	1.25824
0.8593	0.93272	0.90135	1.61837
0.8024	0.88667	0.82884	2.17428
0.7247	0.81893	0.72872	2.99351
0.6588	0.75491	0.64702	3.59277
0.6586	0.75205	0.64403	3.59460
0.6357	0.73091	0.61928	3.76875
0.6354	0.72918	0.61748	3.77095
0.5388	0.62700	0.51373	4.25274
0.5388	0.63264	0.51948	4.25280
0.5053	0.59814	0.48927	4.31276
0.5050	0.59147	0.48256	4.31306
0.4817	0.57199	0.46734	4.32272
0.3914	0.46851	0.38605	4.17185
0.3497	0.41597	0.34630	3.99836
0.3117	0.36480	0.30753	3.79321
0.2596	0.29257	0.25271	3.46230
0.2137	0.22537	0.20055	3.13128
0.1739	0.16586	0.15326	2.81257
0.1498	0.12846	0.12227	2.60537